

NAVAL POSTGRADUATE SCHOOL Monterey, California



THESIS

HOLLOW CATHODE PLASMA SOURCE
CHARACTERISTICS

by

Park, Young-chul

December 1989

Thesis Advisor

Richard Christopher Olsen

Approved for public release; distribution is unlimited.

Unclassified

security classification of this page

| REPORT DOCUMENTATION PAGE | | | |
|---|---|---|---|
| 1a Report Security Classification Unclassified | | 1b Restrictive Markings | |
| 2a Security Classification Authority | | 3 Distribution Availability of Report | |
| 2b Declassification Downgrading Schedule | | Approved for public release; distribution is unlimited. | |
| 4 Performing Organization Report Number(s) | | 5 Monitoring Organization Report Number(s) | |
| 6a Name of Performing Organization Naval Postgraduate School | 6b Office Symbol <i>(if applicable)</i> 33 | 7a Name of Monitoring Organization Naval Postgraduate School | |
| 6c Address <i>(city, state, and ZIP code)</i> Monterey, CA 93943-5000 | | 7b Address <i>(city, state, and ZIP code)</i> Monterey, CA 93943-5000 | |
| 8a Name of Funding Sponsoring Organization | 8b Office Symbol <i>(if applicable)</i> | 9 Procurement Instrument Identification Number | |
| 8c Address <i>(city, state, and ZIP code)</i> | | 10 Source of Funding Numbers | |
| | | Program Element No | Project No Task No Work Unit Accession No |
| 11 Title <i>(include security classification)</i> HOLLOW CATHODE PLASMA SOURCE CHARACTERISTICS | | | |
| 12 Personal Author(s) Park, Young-chul | | | |
| 13a Type of Report Master's Thesis | 13b Time Covered From To | 14 Date of Report <i>(year, month, day)</i> December 1989 | 15 Page Count 65 |
| 16 Supplementary Notation The views expressed in this thesis are those of the author and do not reflect the official policy or position of the Department of Defense or the U.S. Government. | | | |
| 17 Cosati Codes | | 18 Subject Terms <i>(continue on reverse if necessary and identify by block number)</i> | |
| Field | Group | Subgroup | Hollow cathode plasma source |
| | | | |
| | | | |
| 19 Abstract <i>(continue on reverse if necessary and identify by block number)</i> | | | |
| <p>The experimental and theoretical research results on plasma and its sources are presented. This work involves characterizations of useful qualitative descriptions of the basic physical processes taking place within a vacuum chamber and hollow cathode. The purpose of this experiment is to determine the minimum operating power and stable conditions of a standard, commercial hollow cathode plasma source. The results of this experiment will be compared with the results produced by other plasma laboratories.</p> | | | |
| 20 Distribution Availability of Abstract | | 21 Abstract Security Classification | |
| <input checked="" type="checkbox"/> unclassified unlimited <input type="checkbox"/> same as report <input type="checkbox"/> DTIC users | | Unclassified | |
| 22a Name of Responsible Individual Richard Christopher Olsen | | 22b Telephone <i>(include Area code)</i> (408) 646-2019 | 22c Office Symbol 610s |

Approved for public release; distribution is unlimited.

Hollow Cathode Plasma Source
Characteristics

by

Park, Young-chul
Lieutenant, Republic of Korea Navy
B.S.E.E., Korean Naval Academy, 1982

Submitted in partial fulfillment of the
requirements for the degree of

MASTER OF SCIENCE IN PHYSICS

from the

NAVAL POSTGRADUATE SCHOOL
December 1989

Author:



Park, Young-chul

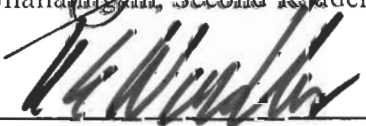
Approved by:



Richard Christopher Olsen, Thesis Advisor



S. Gnanalingam, Second Reader



Karlheinz E. Wochler, Chairman,
Department of Physics

ABSTRACT

Experimental and theoretical research results on plasma and its sources are presented. This work involves characterization of the basic physical processes taking place with a hollow cathode within a vacuum chamber. The purpose of this experiment is to determine the minimum operating power and stable conditions of a standard, commercial hollow cathode plasma source. The results of this experiment will be compared with the results produced by other plasma laboratories.

TABLE OF CONTENTS

| | | |
|-----|---|----|
| I. | INTRODUCTION | 1 |
| II. | THEORIES AND CHARACTERISTICS OF VARIOUS CATHODES | 3 |
| A. | HOLLOW CATHODE | 3 |
| 1. | HOLLOW CATHODE WITH HEATER | 3 |
| a. | CONSTRUCTION | 3 |
| b. | OPERATING CHARACTERISTICS | 6 |
| 2. | HOLLOW CATHODE WITHOUT HEATER | 10 |
| a. | CONSTRUCTION | 10 |
| b. | OPERATING CHARACTERISTICS | 10 |
| 3. | HOLLOW CATHODE LAMP | 12 |
| a. | CONSTRUCTION | 12 |
| b. | OPERATING PRINCIPLE AND CHARACTERISTICS | 15 |
| 4. | RELATIVISTIC ELECTRON BEAM SOURCE | 17 |
| a. | CONSTRUCTION | 17 |
| b. | OPERATING PRINCIPLE AND CHARACTERISTICS | 18 |
| B. | HOLLOW CATHODE THEORY | 19 |
| C. | LANGMUIR PROBE | 21 |
| D. | THE DEFINITION OF IGNITED DISCHARGE MODE | 23 |

| | | |
|------|---|----|
| III. | APPARATUS | 25 |
| | A. DISCHARGE CHAMBER | 25 |
| | B. ELECTRICAL CIRCUIT | 27 |
| | C. MEASURING EQUIPMENT | 27 |
| | D. VACUUM SYSTEM | 28 |
| IV. | OPERATING PROCEDURE | 29 |
| V. | EXPERIMENTAL RESULTS | 32 |
| | A. POSITIVE ANODE POTENTIAL RELATIVE TO KEEPER | 32 |
| | B. NEGATIVE ANODE POTENTIAL RELATIVE TO KEEPER | 35 |
| | C. ANODE GEOMETRY DEPENDENCE | 37 |
| | D. CATHODE TO KEEPER DISTANCE DEPENDENCE WITH MESH COLLECTOR | 39 |
| | E. HEATER DEPENDENCE | 42 |
| | F. ELECTRON TEMPERATURE AND DENSITY | 43 |
| | G. OTHER RESULTS | 46 |
| VI. | FURTHER WORK | 48 |
| VII. | CONCLUSIONS | 50 |
| | REFERENCES | 52 |
| | INITIAL DISTRIBUTION LIST | 54 |

LIST OF FIGURES

| | | |
|-----------|---|----|
| Fig. 2.1 | Hollow cathode configurations | 3 |
| Fig. 2.2 | Orifice configurations | 5 |
| Fig. 2.3 | Internal electrode configuration | 5 |
| Fig. 2.4 | Discharge initiation data for cathode with tubular insert | 6 |
| Fig. 2.5 | Discharge initiation data for cathode with rolled foil insert | 7 |
| Fig. 2.6 | Discharge initiation characteristics of curved orifice cathode | 8 |
| Fig. 2.7 | Comparison of discharge behavior with different orifices | 9 |
| Fig. 2.8 | Internal electrode discharge initiation characteristics | 10 |
| Fig. 2.9 | Heaterless hollow cathode configurations | 10 |
| Fig. 2.10 | Voltage – current characteristic of Spectra – Mat cathode | 12 |
| Fig. 2.11 | Construction of hollow cathode lamp | 13 |
| Fig. 2.12 | Starting potential as a function of pd_s in several gases | 15 |
| Fig. 2.13 | Schematic of ionization process | 16 |
| Fig. 2.14 | Current – voltage curve | 17 |
| Fig. 2.15 | Simple foilless electron beam source with applied magnetic field | 18 |

| | | |
|-----------|--|----|
| Fig. 2.16 | Typical orificed, hollow cathode | 20 |
| Fig. 2.17 | Schematic of ion production region | 20 |
| Fig. 2.18 | Current – voltage characteristics of a Langmuir probe | 22 |
| Fig. 2.19 | i_e vs. probe potential curve | 23 |
| Fig. 2.20 | Characteristic of ignited mode | 24 |
| Fig. 3.1 | General experimental apparatus | 25 |
| Fig. 3.2 | Inside the vacuum chamber | 26 |
| Fig. 3.3 | Electrical circuit | 27 |
| Fig. 3.4 | Varian vacuum system | 28 |
| Fig. 4.1 | Aging effect of cross section of a orifice | 30 |
| Fig. 4.2 | plasma potential distribution inside the chamber | 30 |
| Fig. 5.1 | Geometry of experimental arrangement | 32 |
| Fig. 5.2 | Discharge voltage vs. flow rate | 33 |
| Fig. 5.3 | Discharge voltage vs. anode accelerating potential | 33 |
| Fig. 5.4 | Level off potentials | 34 |
| Fig. 5.5 | Bias configuration | 36 |
| Fig. 5.6 | Discharge voltage vs. anode to cathode potential | 36 |
| Fig. 5.7 | Anode current vs. potential | 37 |
| Fig. 5.8 | Mesh shield anode and vacuum chamber geometry | 37 |
| Fig. 5.9 | Discharge voltage vs. anode potential | 38 |
| Fig. 5.10 | Anode current vs. anode potential | 39 |
| Fig. 5.11 | Discharge voltage vs. anode potential for $I_k = 2.0$ A .. | 40 |
| Fig. 5.12 | Discharge voltage vs. anode potential for $I_k = 1.0$ A .. | 41 |
| Fig. 5.13 | Discharge voltage vs. anode potential for flow rate 2.00 sccm | 42 |

| | | |
|-----------|--|----|
| Fig. 5.14 | Probe current vs. potential for normal and ignited discharge mode | 43 |
| Fig. 5.15 | $\ln(i_e)$ vs. probe potential for normal discharge mode ... | 44 |
| Fig. 5.16 | $\ln(i_e)$ vs. probe potential for ignited discharge mode ... | 44 |
| Fig. 5.17 | Summary of electron temperature | 45 |
| Fig. 5.18 | Summary of plasma density | 45 |
| Fig. 5.19 | Chamber pressure variation with respect to discharge states | 46 |
| Fig. 5.20 | Field – enhanced thermionic emission current | 47 |
| Fig. 6.1 | Split mesh anode and bias configuration | 49 |

LIST OF TABLES

| | | |
|-----------|---|----|
| Table 2.1 | Specifications of Spectra – Mat cathode | 11 |
| Table 2.2 | Pt cathode lamp specifications | 14 |
| Table 2.3 | Minimum sparking potentials | 15 |

TABLE OF SYMBOLS

| | |
|-------------|---|
| d | : cathode orifice diameter or cathode to keeper distance |
| e | : electron charge ($1.6 \times 10^{-19} \text{C}$) |
| E | : electric field |
| I | : ionization potential |
| I_o | : electron current to probe in the absence of a retarding field |
| i_a | : anode current |
| i_e | : electron current |
| i_h | : heater current |
| i_i | : ion current |
| i_{is} | : ion saturation current |
| i_k | : keeper current |
| i_p | : Langmuir probe current |
| j_e | : electron current density |
| j_i | : ion current density |
| j_{total} | : total current density |
| K | : Boltzmann constant |
| L_e | : insert emission length |
| m_i | : ion mass |
| n | : plasma density |
| n_a | : density of atom |
| n_i | : ion density |

| | |
|--------------|---|
| p | : gas pressure |
| \dot{q} | : heat loss rate |
| T | : temperature |
| T_e | : electron temperature |
| T_s | : insert emission temperature |
| V_{ac} | : anode to cathode voltage |
| V_{ak} | : anode to keeper voltage |
| V_{Bohm} | : Bohm velocity |
| V_c | : potential drop across the plasma sheath |
| V_f | : floating potential |
| V_i | : ionization potential |
| V_{kc} | : discharge voltage |
| V_l | : potential of Langmuir probe |
| V_s | : sparking potential |
| V_{sp} | : space potential (probe same potential as plasma) |
| ϵ | : emissivity (0.5 for tantalum) |
| ϵ_0 | : permittivity of free space ($8.854 \times 10^{-12} \text{F/m}$) |
| λ_D | : Debye length |
| σ | : Stefan–Boltzmann constant ($5.67 \times 10^{-8} \text{W/m}^2 \cdot \text{K}^4$) |
| ϕ | : work function |
| ϕ_e | : average effective work function |
| ϕ_s | : average surface work function |
| ϕ_w | : charged vacuum chamber wall potential |
| $\bar{\phi}$ | : average work function |

I. INTRODUCTION

Hollow cathode plasma sources are an essential component in ion thrusters, electrothermal launchers, spacecraft neutralizers, heavy particle accelerators and similar devices. A great deal of effort has gone into the development of plasma sources of all kinds in this century and an extensive collection of literature is available on all aspects of plasma source research. Most of this work was done with a view toward high energy accelerators, where typical ion beams have energies of many kilovolts when extracted from the source.

The work presented here is a continuation of studies of the characteristics of a weakly ionized low energy (the order of eV) plasma and its sources. The purpose of this investigation was originally to optimize an argon plasma source with respect to the minimum required operating power and gas flow rate. In the course of the investigation it was discovered that the determination of the characteristics of the plasma and those of the cathode were complicated because some variables such as electron temperature, plasma density, and the properties of the hollow cathode interior were hard to determine accurately. Therefore, some of these variables are quoted from other material that was published by other plasma investigations. [Ref. 1]

The literature survey which follows was designed to consider the broad spectrum of hollow cathode discharge devices. This include designs for ion engines, as well as UV sources. The laboratory investigation was then directed toward a study of the external effects, how the characteristics of the plasma and its source varied with gas flow rate, electric field, the separation distance from the cathode tip

to keeper, types of cathode, etc.. To prevent the problems associated with opening the vacuum chamber, a cathode mount was designed for variable cathode – anode separation using a motor drive.

The designed cathode and Langmuir probe device achieved operational status late in the period allotted for research and only a cursory look at the variable cathode tip to keeper distance effects was achieved.

II. THEORIES AND CHARACTERISTICS OF VARIOUS CATHODES

Here the basic principles of ionization, gas discharge, Langmuir probe theories and the broad survey results of hollow cathodes will be discussed.

A. HOLLOW CATHODE

1. HOLLOW CATHODE WITH HEATER

a. CONSTRUCTION

Most of the electron bombardment plasma sources employ a hollow cathode. Variety of cathodes have generally similar shapes as shown in Figure 2.1.

[Ref. 11]

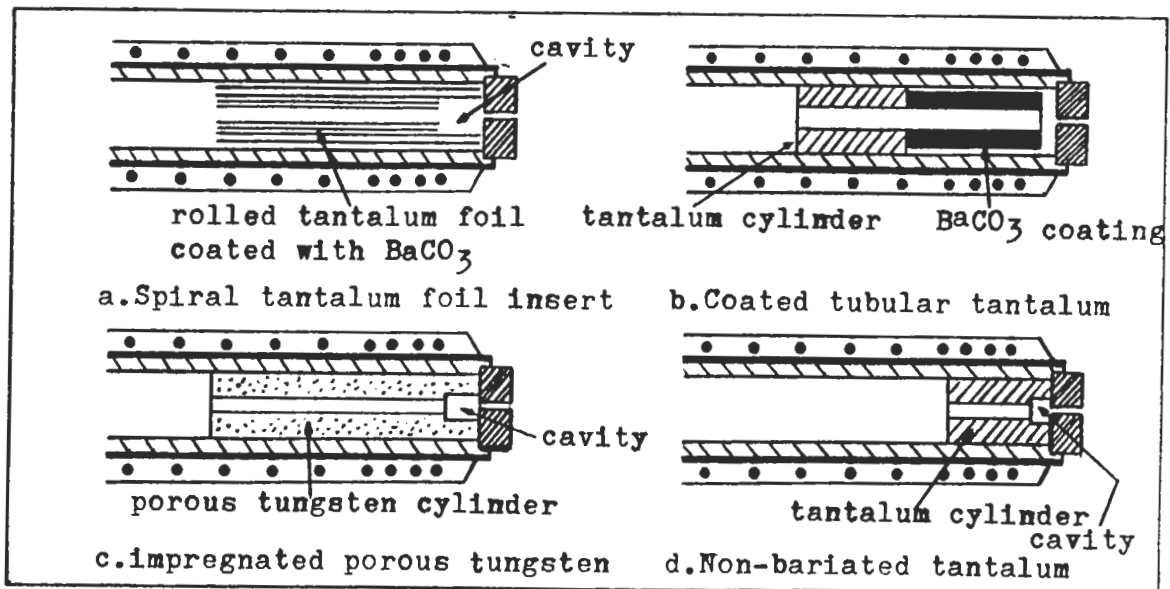


Figure 2.1 hollow cathode configurations [Ref. 11]

General constructions are as follows:

(1) Cathode body and tip

The body and tip consist of tantalum tube into one end of which is welded a 1 mm thick tungsten disc containing an orifice. On occasion, the tube and tip were made of molybdenum to simplify the fabrication of special orifice shapes. The outside diameter of the tube is generally 3.2 mm (1/8") or 7 mm (1/4") with a wall thickness from 0.2 mm to 0.5 mm.

(2) Cathode heater

Surrounding the tube at its orifice side end is a spiral heater wire encapsulated in a ceramic material. The wire is generally 0.2 mm diameter pure tungsten, but tungsten/3 % rhenium is sometimes used.

(3) Barium source

Most hollow cathodes contain a source made of a low work function material, such as barium, ostensibly to improve their thermionic emission capabilities. There are essentially four methods of applying the barium to the source.

(a) coating the inner wall of the cathode body.

(b) coating a thin strip of tantalum foil which is then rolled into a spiral on a mandrel before being inserted into the cathode body.

(c) coating the inner or outer surface of a cylindrical metal insert.

(d) the impregnation of a porous metal insert. It was also reported that the operation of cathode without low work function material was possible. [Ref.11]

(4) Orifice plate and orifice

The orifice diameters are a few tenths to one millimeter and the purpose of the orifice plate is to improve the ionization probability by

increasing the number density of the propellant gas inside the cathode. There are two typical orifice configurations. One is a straight cylindrical hole and the other is curved one as shown in Figure 2.2. It was found that the discharge characteristic of the curved orifice was better than the characteristic for a cylindrical orifice in same condition.

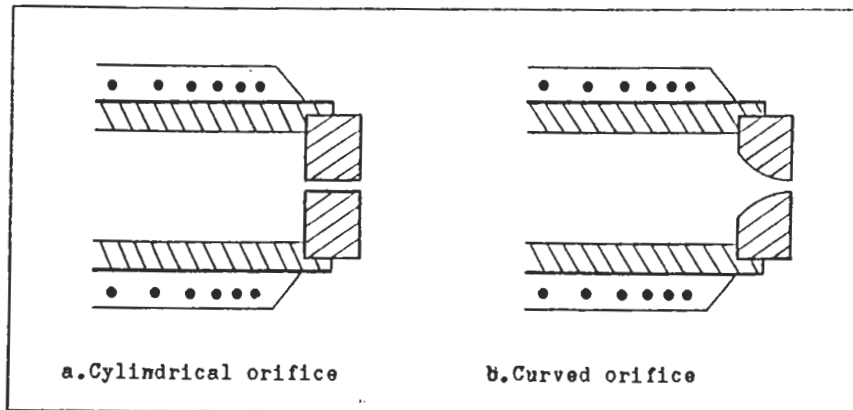


Figure 2.2 Orifice configurations

(5) Auxiliary electrode

The early stages of hollow cathode studies included the use of internal auxiliary electrode as shown in Figure 2.3. The tip of an internal electrode was usually positioned about 2 mm from the internal face of orifice plate. This electrode supported the initiation of discharge. Such electrodes are rarely used for discharge initiation now, but can be used as a Langmuir probe to investigate processes inside the cathode.

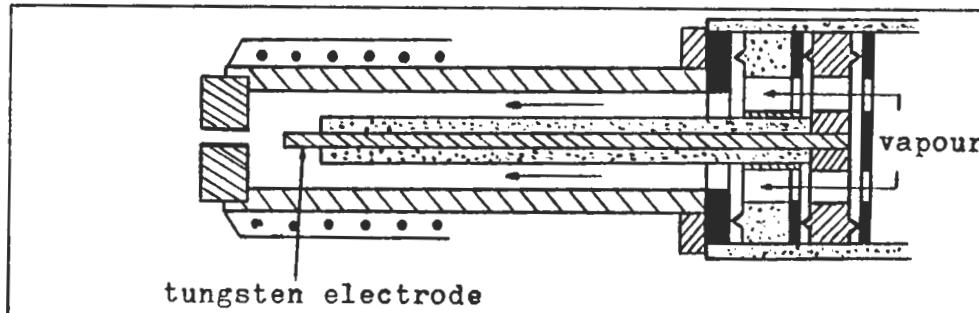


Figure 2.3 Internal electrode configuration [Ref. 11]

b. OPERATING CHARACTERISTICS

One of the most critical characteristics of hollow cathodes are their starting behavior. The variables related to starting behavior are complex, but here the effects of gas flow rate, heater temperature and cathode to keeper potential will be considered. Two of the four designs illustrated above (Fig. 2.1) are each considered here.

(1) Cathode with tubular insert

The inner surface of the cylindrical metal insert is coated with a controlled quantity of carbonates. For an orifice diameter of 0.3 mm and a flow rate 4.03 sccm, discharge initiation was possible from 1000°C to 1350°C. Voltages were well below 50 V, with values as low as 15 V being recorded. The full results are shown in Figure 2.4. To be completely sure of obtaining a discharge, it was necessary to apply 350 V, at 1150°C, 150 V at 1200°C and 40 V at 1300°C. For higher flow rates, the starting voltages were lowered, but the sensitivity to flow rate was not so great as the sensitivity to temperature. The lowest operating temperature for a flow rate of 4.03 sccm was about 900°C. [Ref. 11]

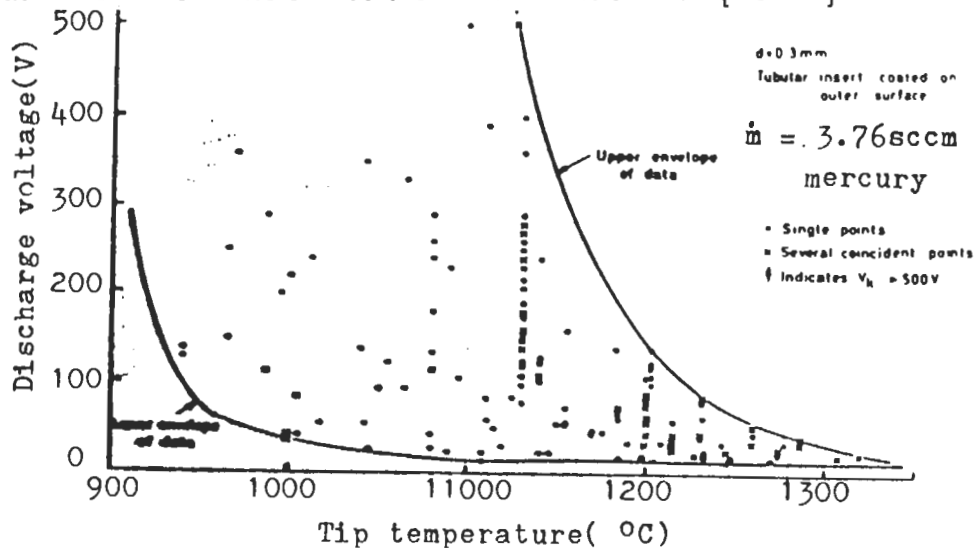


Figure 2.4 Discharge initiation data for cathode with tubular insert [Ref. 11]

(2) Rolled foil insert

In this case, the insert is fabricated by coating a thin strip of tantalum foil which is then rolled into a spiral on a mandrel before being inserted into the cathode body. This is more susceptible to vibration damage than the tubular insert. It was found that discharge initiation occurred at much lower temperatures with this cathode than the tubular insert, but that the general behavior was qualitatively similar. For a flow rate of 4.03 sccm, starting was possible at below 800°C. Full results for flow rate 3.36 sccm are shown in Figure 2.5. [Ref. 11]

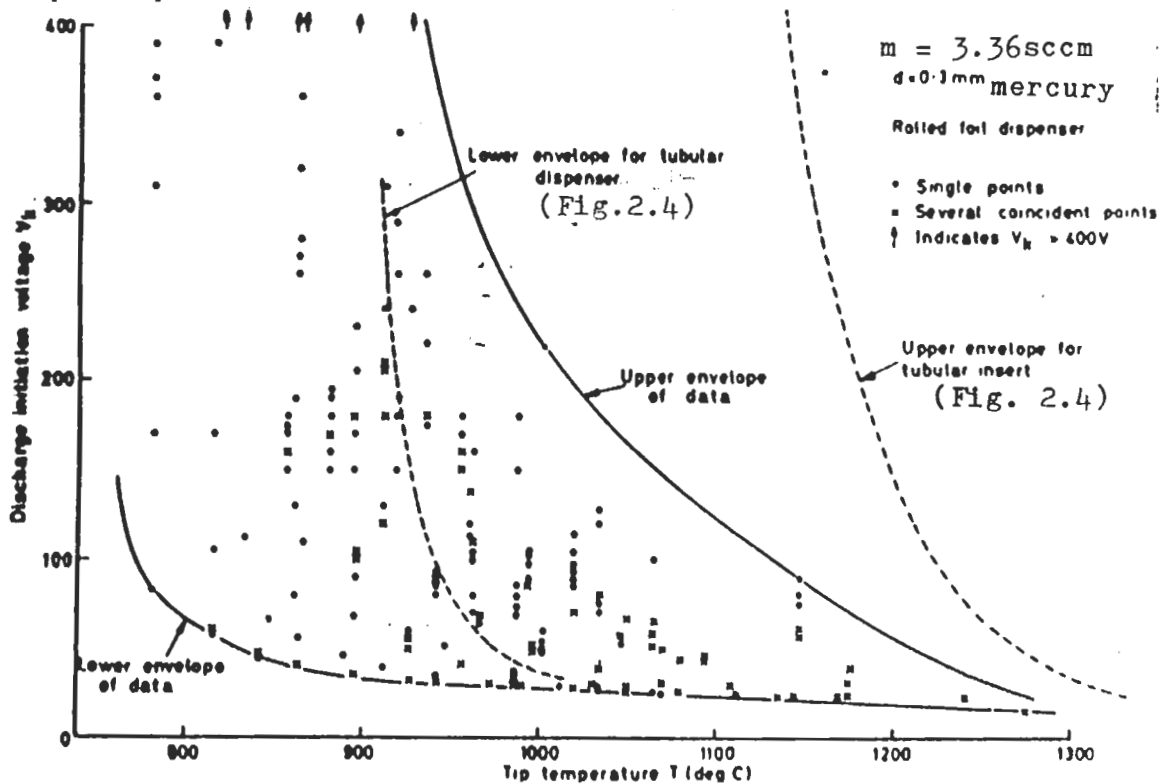


Figure 2.5 Discharge initiation data for cathode with rolled foil insert [Ref. 11]

(3) Curved orifice cathode

Modifying the orifice plate by using a curved orifice resulted in extremely good starting characteristics. Qualitatively, the behavior was similar

to that observed before, but values for the starting voltage were lower. This might be due to better penetration of the electric field through the orifice, or better gas/ion transport through the orifice. Such ease of starting had not been observed before. However, the plume to spot mode transition was unstable. Full results for two flow rates are shown in Figure 2.6. [Ref. 11]

(4) Non-bariated cathode

It is possible to operate a hollow cathode containing no low work function material, with some changes in performance. This cathode required very much higher tip temperature for normal operation, usually 200°C higher than with a bariated cathode. A flow rate of 16.8 sccm had to be adopted as standard to enable the non-bariated cathode to be started at temperatures within the capability of its heater. [Ref. 11]

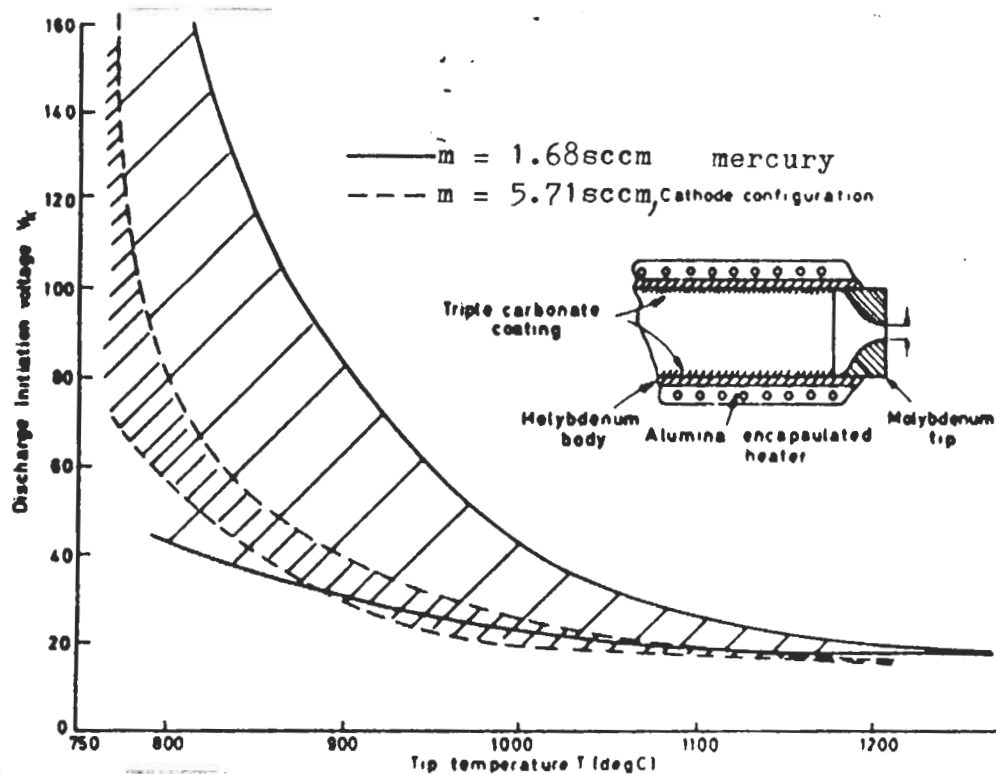


Figure 2.6 Discharge initiation characteristics of curved orifice cathode [Ref. 11]

(5) Effect of orifice diameter

For the orifice diameter 0.15 mm and 0.3 mm and flow rates 16.8 sccm to 20.2 sccm, the starting characteristics are shown in Figure 2.7. These indicate that a change in diameter produced less effect than any other variables.

(6) Auxiliary electrode

An auxiliary electrode can be used to initiate the discharge. For positive electrode potential, it was found that an internal discharge could be initiated at low voltages. As illustrated in Figure 2.8 these were often below the ionization potential (10.437 V for mercury) for values of temperature ranging from about 600°C to 1200°C. With temperature 1200°C and flow rate 2.69 sccm, a potential of only 6 V was required to start the discharge. However, it was found very difficult to transfer the internal discharge to the keeper, possibly because the electric field in the cathode orifice due to the keeper was opposed by that due to the positive internal electrode. [Ref. 11]

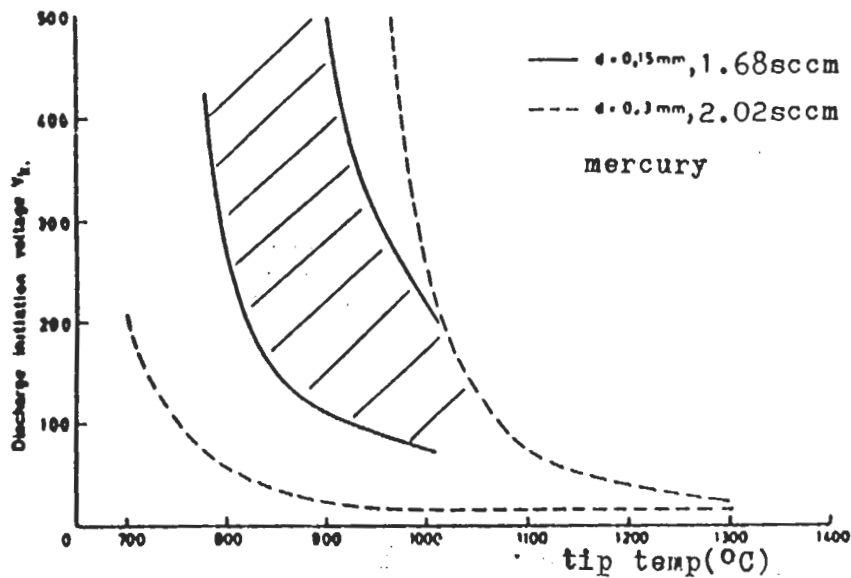


Figure 2.7 Comparison of discharge behavior with different orifices [Ref. 11]

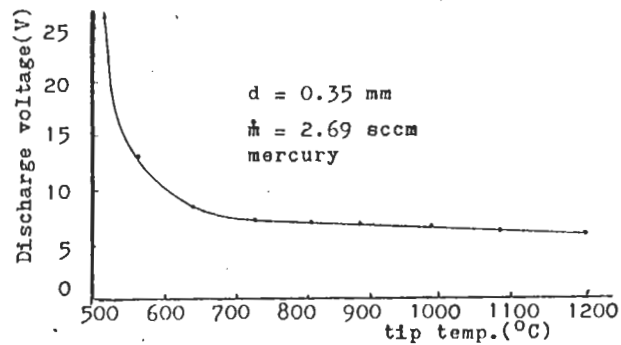


Figure 2.8 Internal electrode discharge initiation characteristics [Ref. 11]

2. HOLLOW CATHODE WITHOUT HEATER

a. CONSTRUCTION

It is possible to design a hollow cathode without a heater. In Figure 2.9, interior (cathode wrapped by cylindrical keeper) and exterior (cathode exposed) heaterless hollow cathode are shown.

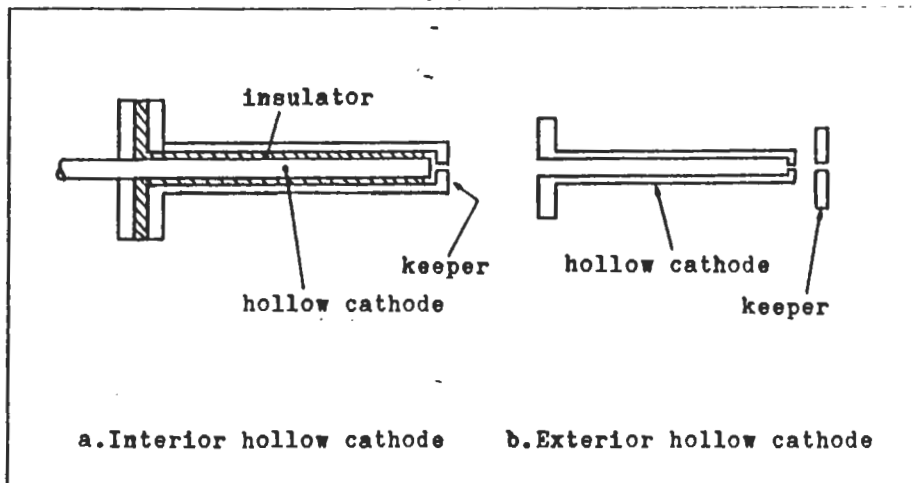


Figure 2.9 Heaterless hollow cathode configurations

b. OPERATING CHARACTERISTICS

Heaterless cathodes utilize Paschen's law without the support of thermal emission. Heaterless cathodes are relatively simple, robust and need much lower power to operate. Some of advantages are

- (1) longer cathode life time
- (2) more robust
- (3) lower power consumption
- (4) less chance of ion beam and substrate contamination

disadvantages are

- (1) relatively high starting potential required
- (2) hard to control contamination.

One commercially available "interior" cathode design (Fig. 2.9) has the characteristics listed in Table 2.1. Operating characteristics are illustrated in Figure 2.10. [Ref. 12]

Table 2.1 Specifications of Spectra – Mat cathode

| | |
|---------------------------|----------------------|
| starting time | : 10 secs |
| emission current | : 0 – 10 A |
| gas flow requirements | : 1.0 – 5.0 sccm |
| life time | : 500 – 1000 hrs |
| power requirements | |
| start | : 270 VDC 0.5 A |
| run | : 7 – 10 VDC 1.0 A |
| power supply requirement: | 115 +/- 15 VAC 60 Hz |
| | 36 VDC 1.7 A |
| | 240 VDC 0.5 A |
| anode supply | : 50 – 100 VDC |
| | 0.7 A |

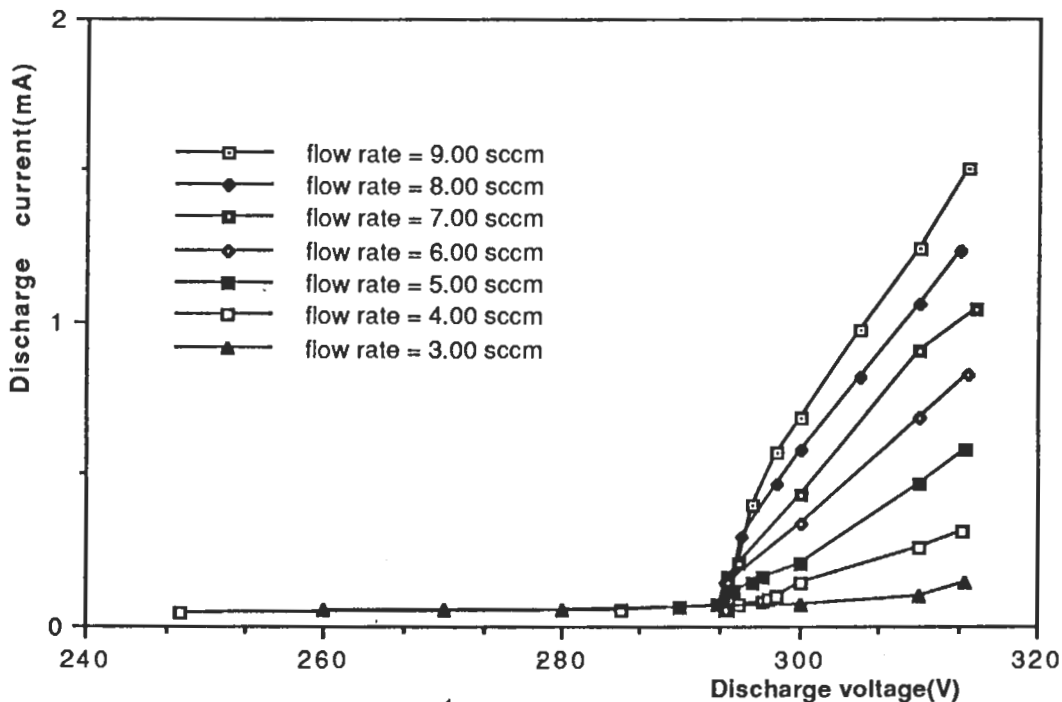


Figure 2.10 Voltage – current characteristic of Spectra – Mat cathode

3. HOLLOW CATHODE LAMP

Enclosed cathodes (without continuous gas flow) are used as light sources. As an example, let us consider a compact hollow cathode lamp which was developed for use as a high resolution wavelength standard for ultraviolet emission. Simply this is a small two electrode vacuum tube with relatively high gas pressure (the order of torr).

a. CONSTRUCTION

A hollow cathode lamp, as shown in Figure 2.11, is constructed with a bulb having a window made of UV transmitting glass. The gas within the bulb consists of a rare gas at several torr pressures. The cathode is constructed of a single element or alloy of the element to be analyzed so as to ensure a sharp

spectral line with a minimum of intensity spectral components. Typical cathode materials are Fe, Ni, Cu, Ru, Ge, Se, Pt and their alloys.

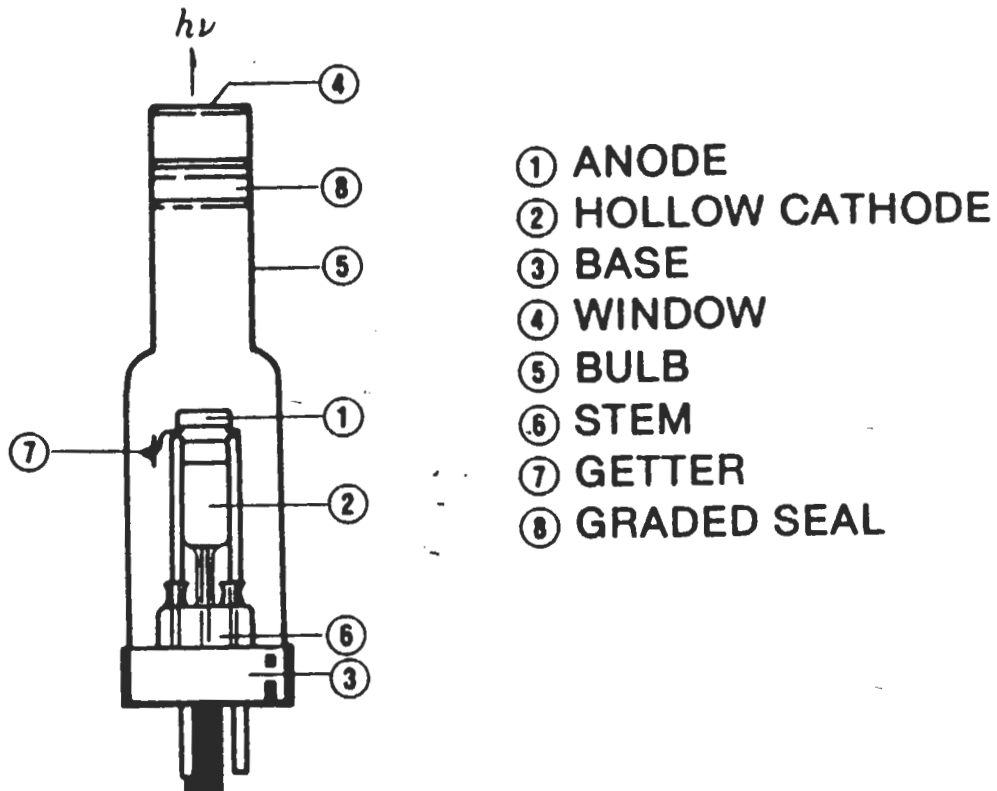


Figure 2.11 Construction of hollow cathode lamp [Ref. 10]

Such lamps are commercially available. As an example, we used one which was available at NPS. This lamp had a platinum cathode, filled with a neon gas at a pressure of 11 torr. This design has a rich spectrum below 3100 \AA . Specifications are given in Table 2.2. [Ref. 9 & 10]

Table 2.2 Hamamatsu Pt cathode lamp specifications

| | |
|-----------------------|---------------------|
| A. Overall Dimensions | |
| length | : 19.70 cm |
| diameter | : 4.45 cm |
| mass | : 285 g (potted) |
| | : 71 g (not potted) |
| cathode – lens | |
| distance | : 8.57 cm |
| B. Cathode | |
| material | : platinum |
| outside diameter | : 0.64 cm |
| inside diameter | : 0.229 cm |
| length | : 0.8 cm |
| hole depth | : 0.41 cm |
| mass | : 4.0 g |
| filler gas | : neon at 11 torr |
| C. Power requirements | |
| starting voltage | : 300 V |
| operating voltage | : 185 V |
| current | : 10 – 60 mA |
| operating power | : 2 W at 10 mA |

The starting voltage of 300 V, neon gas pressure at 11 torr, and a cathode to anode distance of a few millimeters gives a pd_s (about 5 mmHg·cm) which agrees with Paschen's law. Figure 2.12 and Table 2.3 show the Paschen's curve and minimum discharge starting potential for a number of gases and cathode materials. [Ref. 13]

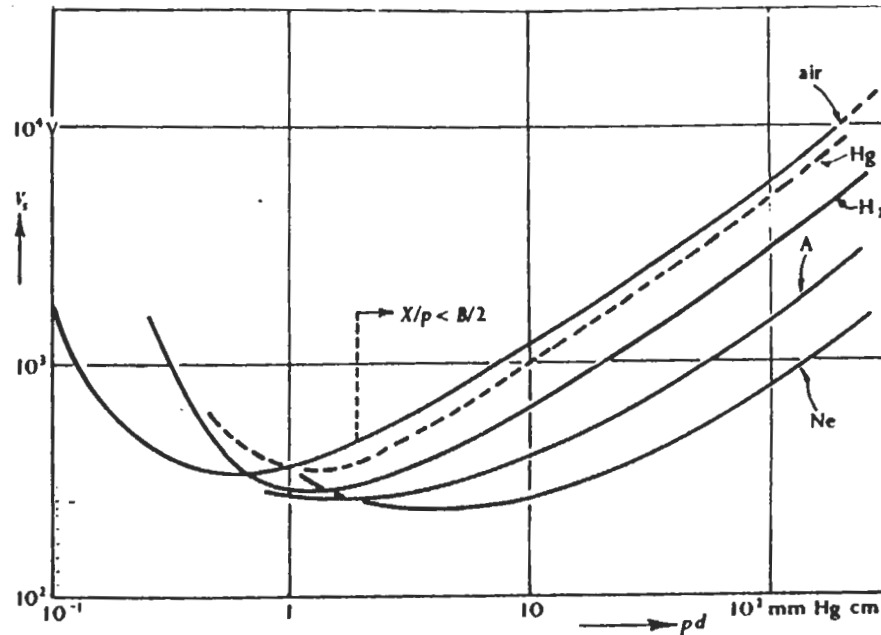


Figure 2.12 Sparking potential as a function of pd_s in several gases [Ref. 13]

b. OPERATING PRINCIPLE AND CHARACTERISTICS

The hollow cathode lamp is a type of glow discharge tube. The electrode construction has been designed to increase the negative glow portion current density, thereby achieving a high emitted spectral intensity for use as a high resolution wavelength standard. [Ref. 9 & 10]

The usual method of increasing the current density is to employ a hollow cathode. This results in a ten – fold or greater increase in current density over that achievable by using a parallel plate electrode. This increase in current density is accompanied by a significant increase in light intensity and a decrease in anode to cathode voltage drop. This is known as the hollow cathode effect. [Ref. 9]

Table 2.3 Minimum sparking potentials [Ref. 13]

| Gas | Cathode | V_{\min} (V) | $(pd_s)_{\min}$ (mmHg·cm) |
|-----|---------|----------------|---------------------------|
| He | Fe | 150 | 2.5 |
| Ne | Fe | 244 | 3 |
| A | Fe | 265 | 1.5 |

(table continued)

| | | | |
|-----------------|----|-----|------|
| N ₂ | Fe | 275 | 0.75 |
| O ₂ | Fe | 450 | 0.7 |
| Air | Fe | 330 | 0.57 |
| H ₂ | Pt | 295 | 1.25 |
| CO ₂ | | 420 | 0.5 |
| Hg | W | 425 | 1.8 |
| Hg | Fe | 520 | 2 |
| Hg | Hg | 330 | |
| Na | Fe | 335 | 0.04 |

According to Paschen's discharge law, a glow discharge occurs when a suitable voltage applied between the electrodes of a hollow cathode lamp. Electrons pass from the interior of the cathode to the inner surface of the hollow cathode and flow through the negative glow region towards the anode as shown in Figure 2.13.

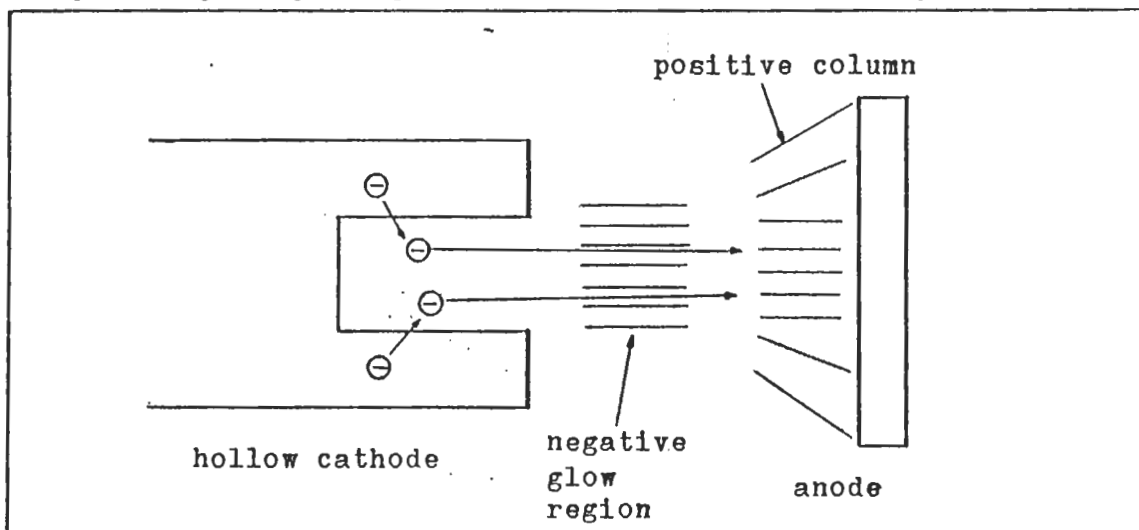


Figure 2.13 Schematic of ionization process

This causes ionization of the gas within the lamp through non – elastic collisions with the gas atoms. Positive gas ions collide with the cathode surface and the kinetic energy of ion impact causes materials to be sputtered from the cathode

surface in the form of an atomic metallic vapor. These metallic atoms collide with the accelerated electrons and are excited. They return to the ground state in an extremely short time (about 10^{-8} sec) and the characteristic monochromatic light of the element is emitted. The spectral lines for the gas sealed in the lamp may also be observed. Figure 2.14 shows current vs. voltage characteristic curve. When the discharge is in progress, the discharge voltage is maintained at about 200 V which agrees with the hollow cathode effect. [Ref. 10 & 13]

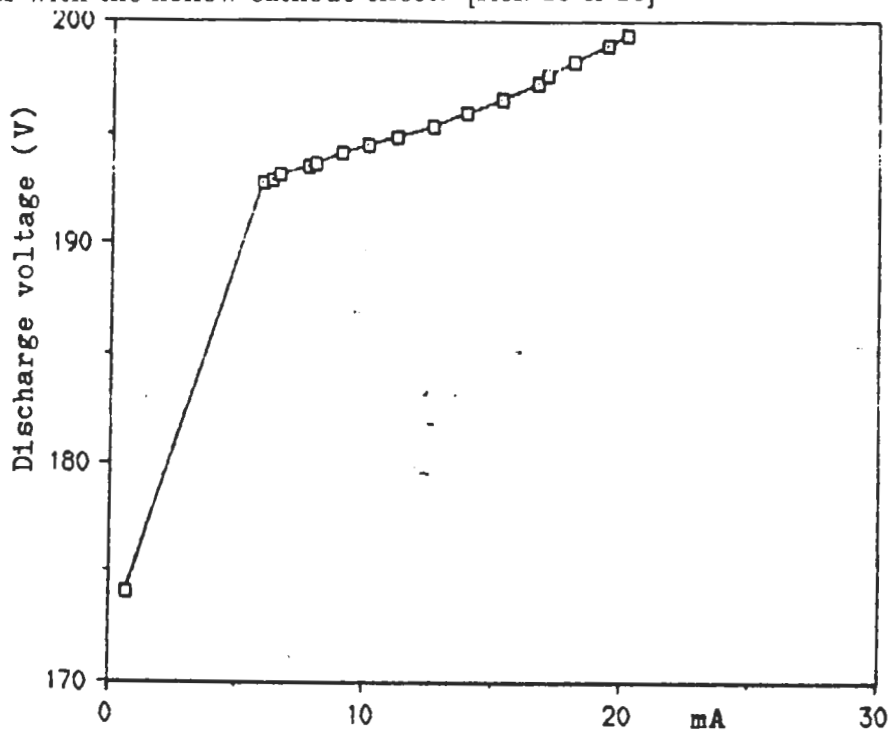


Figure 2.14 Current – voltage curve (measured at NPS)

4. RELATIVISTIC ELECTRON BEAM SOURCE

Hollow cathode designs can be utilized at much higher energies such as electron beam source for Inertial Confinement Fusion driver.

a. CONSTRUCTION

A relativistic electron beam source for an Inertial Confinement Fusion driver consists of hollow cathode, anode and applied magnetic field. A simple foilless electron beam source with magnetic field is shown in Figure 2.15.

This configuration is very similar to the hollow cathode lamp discussed in previous section.

b. OPERATING PRINCIPLE AND CHARACTERISTICS

As expected by its configuration, its principles are similar to the cathode lamp except for its gigantic power requirement. When the high voltage pulse arrives at the cathode, the cathode voltage rises in about 20 ns, and intense field emission occurs from on the cathode surface. The electron beam extracted from the plasma penetrates through the anode and propagates towards the fusion target (pellet).

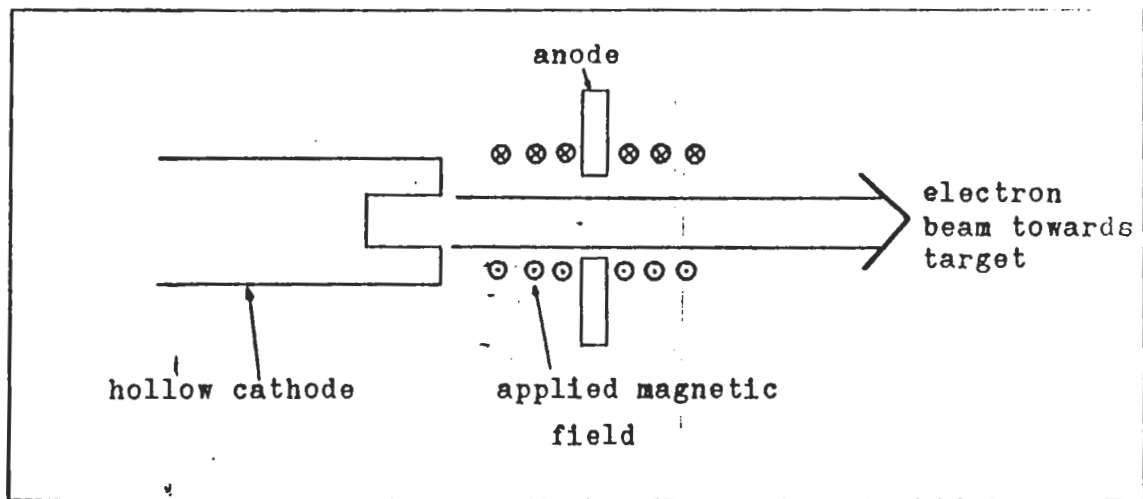


Figure 2. 15 Simple foilless electron beam source with applied magnetic field

The electric field in the electron beam source is about 50 – 100 MV/m, and the beam current density is typically about $10^4 - 10^5$ A/m² (1 – 10 kA/cm²). The equation of electron beam current density is approximately

$$J_e = 1.86 \left[\frac{4\epsilon_0}{9} \right] \times \left[\frac{2e}{m_e} \right]^{-\frac{1}{2}} \frac{\phi^{\frac{3}{2}}}{d_s^{\frac{3}{2}}}$$

The applied magnetic field prevents most of the electrons from striking the anode. Therefore, the voltage drop between anode and cathode can be reduced. [Ref. 15]

B. HOLLOW CATHODE THEORY.

The physical processes which determine hollow cathode behavior are presented next, with an emphasis on the design which utilizes a porous tungsten insert, with heaters. This theory was fully developed by Dan. Siegfried. He explained as follows in " Phenomenological Model Describing Orificed, Hollow Cathode Operation " [Ref. 1]. The orificed, hollow cathode in its simplest form is shown in Figure 2.16.

The cathode consists of an outer refractory metal tube, usually tantalum, covered on its downstream end by an orifice plate usually made of thoriated tungsten. The cathode also normally incorporates a refractory metal insert either coated or impregnated with such chemicals as various barium compounds, which aid the emission process by reducing the work function of the insert surface. Cathodes typically have tube inside diameters of a few millimeters and orifice diameters of a few tenths to one millimeter. The insert length is usually a few times of tube diameter. The electron current is collected by an anode biased positive of the cathode. The keeper acts to maintain a stable discharge in the event of fluctuations in discharge chamber conditions. An external heater is normally used to heat the cathode as aid to start the emission process. However, the process is self – sustaining once the cathode discharge is established and the heater can then be turned off.

The cathode orifice maintains a high neutral density inside the cathode by restricting the propellant flow and it also provides a current path to the downstream discharge. The electron emission comes uniformly from a narrow (about 2 mm) band on the downstream end of the low work function insert and the dominant surface emission process is field – enhanced, thermionic emission. These emitted electrons form 70 % of the total cathode current and the remaining 30 % of the current is due to volume ionization which takes place in the very intense plasma discharge which is established adjacent to the emitting portion of the insert. The important cathode processes are shown schematically in Figure. 2.17. The ions produced in the process leave the production volume at the Bohm velocity and are neutralized at internal cathode potential surface. Ions striking the insert surface provide the energy input which is required to maintain the insert at the emission temperature.

All cathode surfaces which contact the plasma receive ion currents proportional to the Bohm velocity and the plasma density adjacent to the surface. Electron emission, on the other hand, can be assumed to come only from the 2 mm band on the downstream end of the insert. The total emission current (the keeper current plus the anode current) from the cathode is equal to the sum of the ion currents to the various cathode surfaces and the current of the emitted electrons.

Certain aspects of this phenomenological model can be expressed analytically in a simple form which will allow comparison with experimental results. The plasma density adjacent to a particular surface can be calculated based on the Bohm condition using

$$n = \frac{j_i}{eV_{Bohm}} = \frac{I_i}{Ae[KT_e/m_i]^{1/2}} \quad (1)$$

And the total current density to the surface is

$$j_{total} = j_i + j_e \quad (2)$$

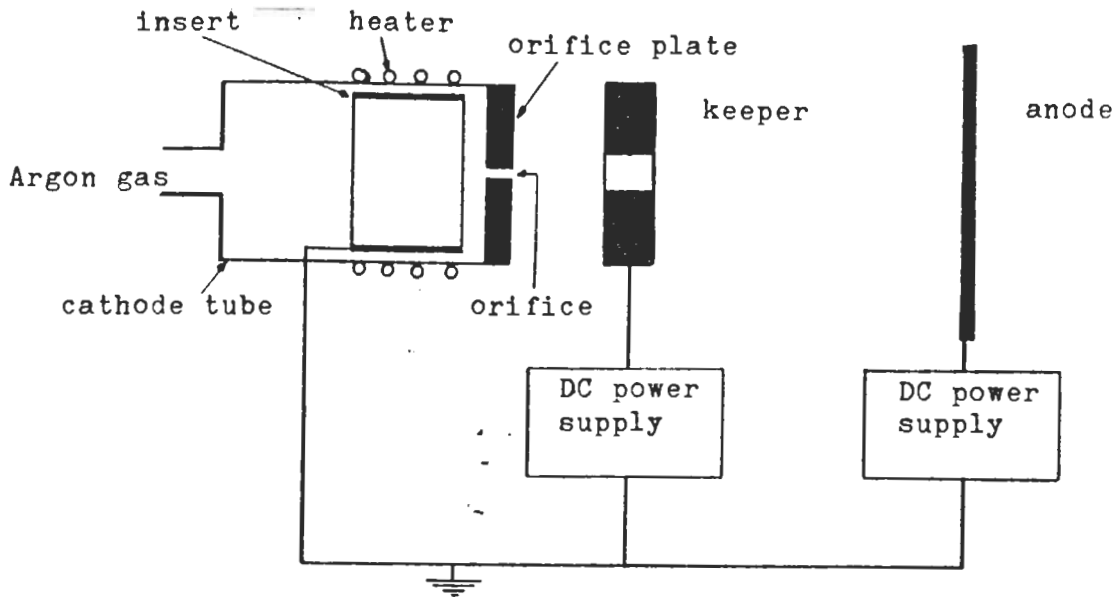


Figure 2.16 Typical orificed, hollow cathode

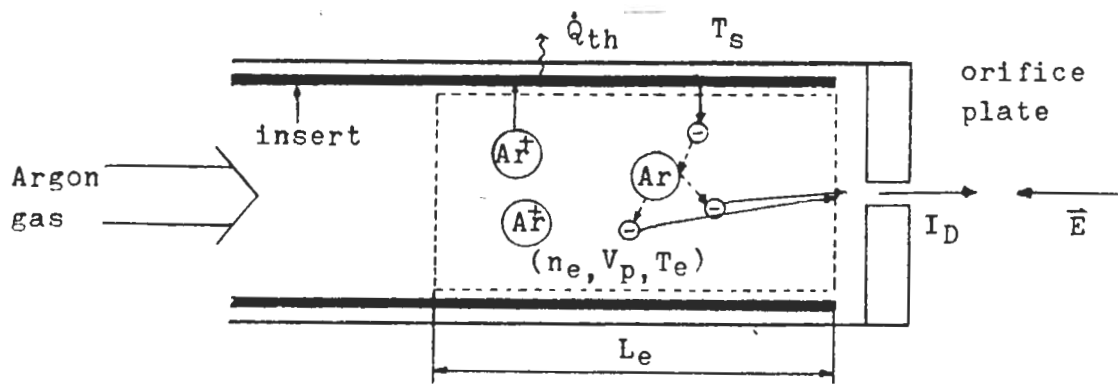


Figure 2.17 Schematic of ion production region

The ratio of ion to electron current can be estimated from an energy balance on the emitting surface. In such a balance the ion heating power is equated to power

conducted and radiated from the surface plus the power required to boil off electrons. The equation describing this is

$$j_e \bar{\phi} + \dot{q} = j_i (V_c + V_i - \phi_s). \quad (3)$$

Equations (5) and (6) can be combined to give the electron emission current density from the surface

$$j_e = \frac{j_{\text{total}} - a\dot{q}}{1 + a\phi_e} \quad (4)$$

$$\text{where } a = (V_c + V_i - \phi_s)^{-1}.$$

The thermal loss can be estimated by the Stefan – Boltzmann law

$$\dot{q} = \epsilon\sigma T^4. \quad (5)$$

Furthermore, the emission from the surface is assumed to be given by the Schottky equation for field – enhanced, thermionic emission

$$j_e = A_0 T^2 \exp[-e\bar{\phi}_e/KT] \quad (6)$$

$$\text{where } A_0 = 120 \text{ A/cm}^2\text{K}^2.$$

The average effective work function $\bar{\phi}_e$ is given by

$$\bar{\phi}_e = \phi_s - \left[\frac{e|E|}{4\pi\epsilon_0} \right]^{-\frac{1}{2}} \quad (7)$$

$$\text{where } E = -\frac{dV}{dX} = -\frac{4}{3} \frac{V_c}{\lambda_D} = -\frac{4V_c}{3} \left[\frac{ne^2}{\epsilon_0 K T_e} \right]^{-\frac{1}{2}}.$$

Here the factor 4/3 comes from Child's law.

This model as it stands does not contain sufficient detail to make predictions of plasma properties or their spatial variation. However, the model can provide an estimate of the insert temperature and this is a critical parameter in determining both the cathode lifetime and performance. [Ref. 1 & 2]

C. LANGMUIR PROBE

The primary diagnostic in the discharge chamber is a Langmuir probe. Typical current – voltage characteristic of a Langmuir probe is shown in Figure 2.18. When the probe is sufficiently negative with respect to the plasma, a positive

ion space charge sheath forms around the probe so that the current collected is the positive ion current, limited by the space charge. This current is termed the saturation ion current i_{is} . As the probe potential becomes less negative with respect to the plasma, electrons with the largest energies can penetrate to the probe and the probe current i_p begins to change as shown in the portion BC of Figure 2.18. The current to the probe i_p is

$$i_p = i_i + i_e \quad (8)$$

A Maxwellian distribution of electron energies is assumed to exist. This allows the response in region BD to be modeled. The fraction of the total electron current which reaches a probe at potential V_1 is $\exp(-eV_1/KT_e)$, where T_e is electron temperature. Then the probe current is

$$i_p = i_i + I_0 \exp(-eV_1/KT_e). \quad (9)$$

Subtracting the ion current, the electron current is obtained

$$i_p - i_i = i_e = I_0 \exp(-eV_1/KT_e). \quad (10)$$

And then take logarithm of equation (10)

$$\ln i_e = \ln I_0 - eV_1/KT_e. \quad (11)$$

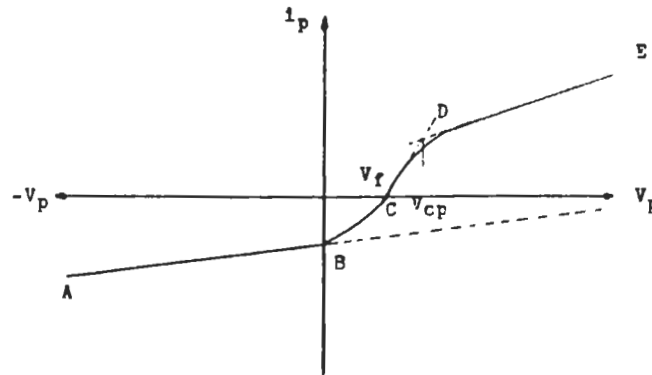


Figure 2.18 Current – voltage characteristic of a Langmuir probe

Thus, assuming the ion current decreases smoothly as the voltage becomes less

negative, the electron current, calculated by subtracting the ion current and its linear extensions from the measured probe current, can be plotted on a semilogarithmic scale vs. the probe potential as Figure 2.19. The slope S on the figure is equal to the value of e/KT_e . Consequently, knowing the slope of the graph, the electron temperature can be determined. Furthermore, if we know the surface area of probe, we can calculate plasma density. [Ref. 5 & 7]

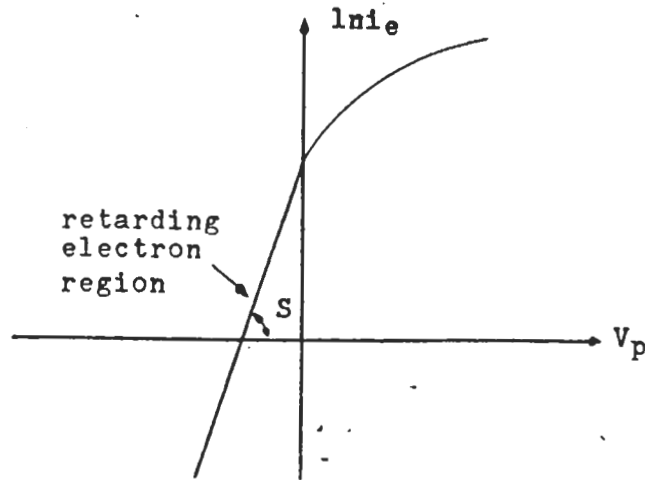


Figure 2.19 i_e vs. probe potential curve

D. THE DEFINITION OF IGNITED MODE

The plasma discharge characteristics can be divided into two special modes in chamber experiments involving current collection. One is the ignited and the other is the normal (unignited) mode. At collector potentials less than about + 80 V (in the NPS chamber) the collected current is relatively low, increasing linearly with voltage. Suddenly, at a collector (anode) potential slightly greater than 80 V, the anode current is shown to increase from 0.05 A to 1 A as shown in Figure 2.20. This transition from a relatively low current collected to a high current is labelled the "transition to ignited mode". The transition is accompanied by the appearance of a bright luminous glow which fills up the whole chamber. This glow could not be seen

in the normal discharge mode. It is suggested that neutral atom excitation (and decay) which induces the luminosity corresponds to ionization of the gas in the chamber. In effect, the collecting grid acts as an anode for the discharge. It was found once in NPS experiments that the discharge between the keeper and cathode moved entirely to the external collecting grid. Once the discharge is operating in the ignited mode small increases in anode potential induce substantial increases in the current. [Ref.18]

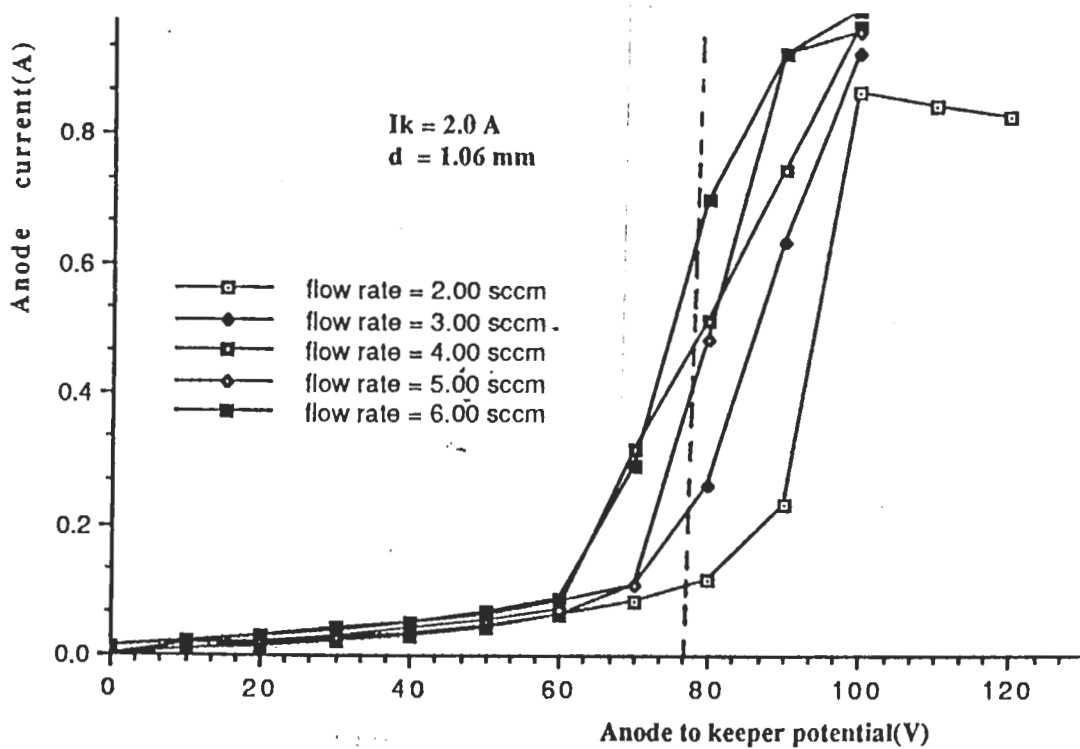


Figure 2.20 Characteristic of ignited mode

III. APPARATUS

The equipment used can be divided into four main components as follows :

1. Discharge chamber and discharge apparatus.
2. Power supplies for the chamber.
3. Measurement instrumentation.
4. Vacuum system.

Figure 3.1 is a photograph of the general experimental arrangement.

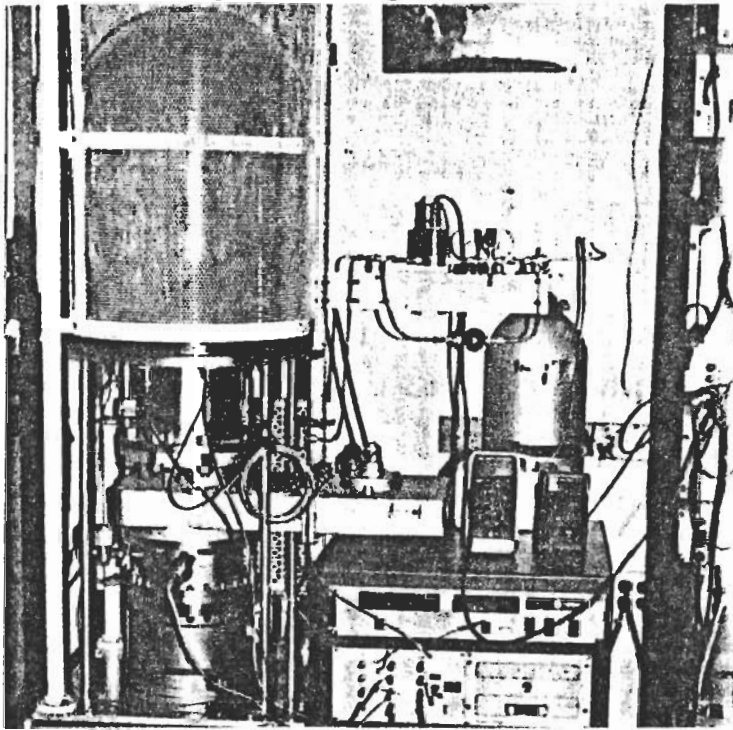


Figure 3.1 General experimental apparatus

A. DISCHARGE CHAMBER

Figure 3.2 is a picture of the chamber system interior. The two electrodes (keeper and mesh type screen), Langmuir probe and two hollow

cathodes (standard and heaterless) were mounted inside the chamber. The standard cathode was purchased from Ion Tech, a manufacturer of equipment for ion deposition. It is based on the NASA/Lewis Research Center design, which is used at Hughes Research Laboratory and Colorado State University. The cathode was mounted so that the interelectrode distance (between keeper and cathode tip) could be varied by a drive motor. This made it possible to vary the device characteristic without opening the vacuum chamber frequently.

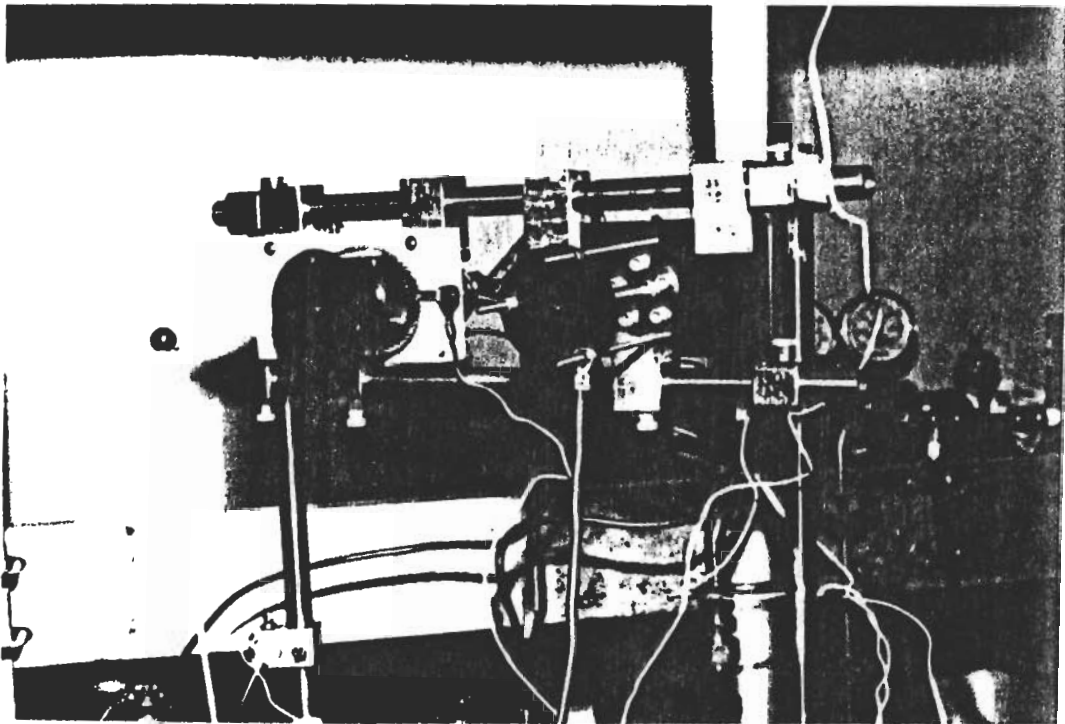


Figure 3.2 Inside the vacuum chamber

The 'heaterless' cathode design is based on Paschen's gas discharge law and was the topic of a different thesis [Ref.16]. Two Langmuir probes (4.765mm and 9.514mm in diameter) were used to measure electron temperature and plasma density. The anode (mesh type screen) was used to collect current and simulate space environmental effects.

Fluke 85 multimeter: measure anode current.

Fluke 75 multimeter: measure keeper current.

Keithley 195A DMM: measure cathode to keeper voltage.

Keithley 485 picoammeter: measure Langmuir probe current.

HP model 120B oscilloscope: usually used to watch system noise and plasma oscillation.

HS – 10S Hasting mass flow transducer and NALL flow meter: measure argon gas flow rate.

D. VACUUM SYSTEM

Figure 3.4 represents the major parts of the Varian vacuum system.

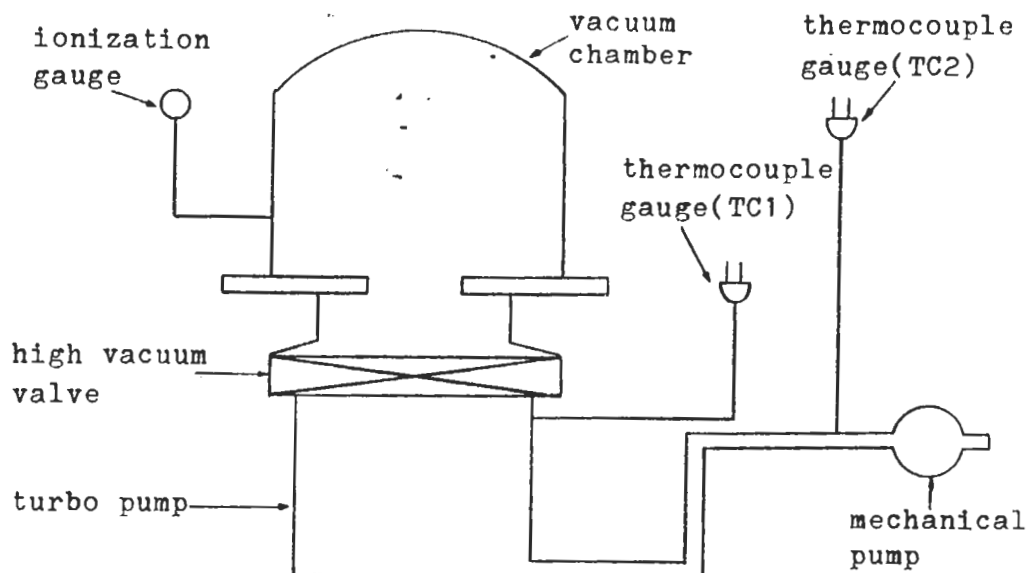


Figure 3.4 Varian vacuum system

The vacuum system consists of two stage pumps and measuring gauges. A rotary vane oil sealed mechanical pump was used as a roughing pump (pressure range: 760 torr to 10^{-3} torr) and a Turbo pump was used as a high vacuum pump (pressure range: 10^{-3} torr to 10^{-8} torr).

IV. OPERATING PROCEDURE

The system should be evacuated to the order of 10^{-6} torr range after opening to insure cleanliness. The system was generally pumped overnight prior to operating, whenever the bell jar had been opened. Argon gas was introduced through the hollow cathode tip where a plasma discharge was initiated by heating cathode tip to about 1000°C . The heater current was turned on at 4 A and then increased to 9 A by 1 A increments at 10 minutes intervals. The flow rate was initially set at 3.00 sccm (the experimentally discovered optimum flow rate to initiate discharge) and a voltage of 300 – 500 VDC was applied to the keeper electrode relative to the cathode. The keeper power supply was designed so that this voltage would drop rapidly to less than 50 V when the keeper discharge started. After a discharge has been established to the keeper, additional electrons can be drawn from the hollow cathode plasma to initiate and sustain the ion source discharge. The heater current which was one of the variables was usually reduced to 6 A. It was possible to set any value between 0 A – 7 A, then set other variables. The variables were keeper current, anode to keeper voltage, gas flow rate, heater current and distance between the cathode tip and keeper. Sometimes bias configurations were changed, that is, anode positive or negative relative to the keeper. [Ref. 14]

The recorded engineering data were keeper current and voltage, anode current and voltage, discharge mode (normal and ignited), gas flow rate and chamber pressure. Langmuir probe traces were run after the system stabilized.

The first efforts were to obtain the system current – voltage characteristics in order to determine the minimum operating power characteristics. This was difficult because the values depended on time and the history of the system. This time dependence was caused by the aging effect of orifice geometry and chamber glass charging. Figure 4.1 shows how the metal has flowed from the outside corners, inward to close the hole. Figure 4.2 shows the potential difference formed by moving electrons with higher mobility than ions. The aging effect could not be controlled. The chamber wall charging was later controlled by adding a mesh type screen anode on the inside wall of the bell jar. [Ref. 7 & 8]

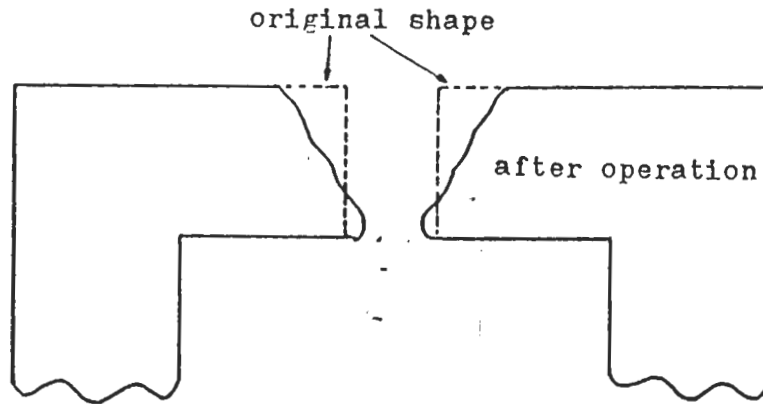


Figure 4.1 Aging effect of cross section of a orifice vacuum chamber wall

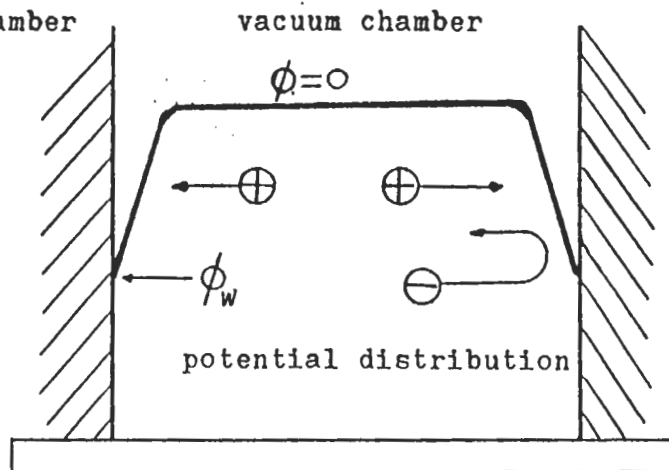


Figure 4.2 Plasma potential distribution inside the chamber

In general, data were recorded when the system approached reasonably fixed values. Otherwise, data were recorded immediately after setting variables, then averaged. Therefore, data, hereafter, are averaged values except a few important cases.

V. EXPERIMENTAL RESULTS

A. POSITIVE ANODE POTENTIAL RELATIVE TO KEEPER

The initial experiments were run with the standard cathode. The keeper was a 1/2 inch diameter piece of tantalum with a 1/4 inch hole. It was mounted 0.25 in. from the cathode. The early stages of the experiments were devoted to determine basic characteristics of the plasma and its source for positive anode potential. During this phase the principal interest was in the determination of efficient discharge conditions. Figure 5.1 shows the geometry of the experimental arrangement. The electric field direction of this arrangement is similar to an ion engine (discharge chamber).

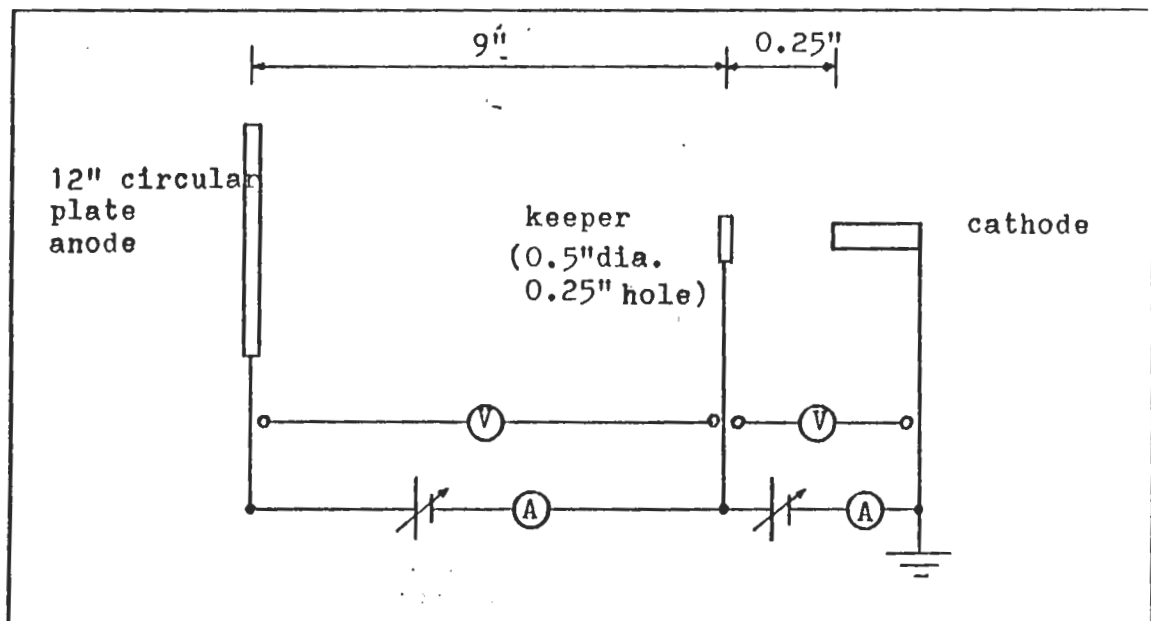


Figure 5.1 Geometry of experimental arrangement

This condition was studied as functions of gas flow rate, total current and anode accelerating potential. Figure 5.2 shows plots of discharge voltage with respect to

flow rate. Discharge potential curve agrees with historical discharge curves . For flow rate less than 3.00 sccm, the discharge voltage depended strongly on the total current. For flow rate higher than 4.00 sccm, the discharge voltages were nearly independent of total current. Figure 5.3 also shows the discharge potential with respect to anode accelerating potential as functions of flow rate. [Ref. 17]

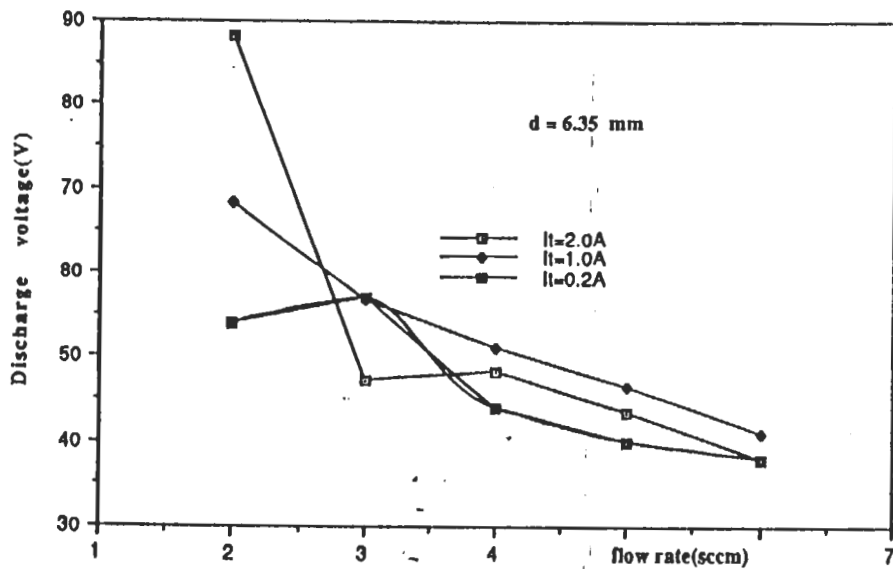


Figure 5.2 Discharge voltage vs. flow rate

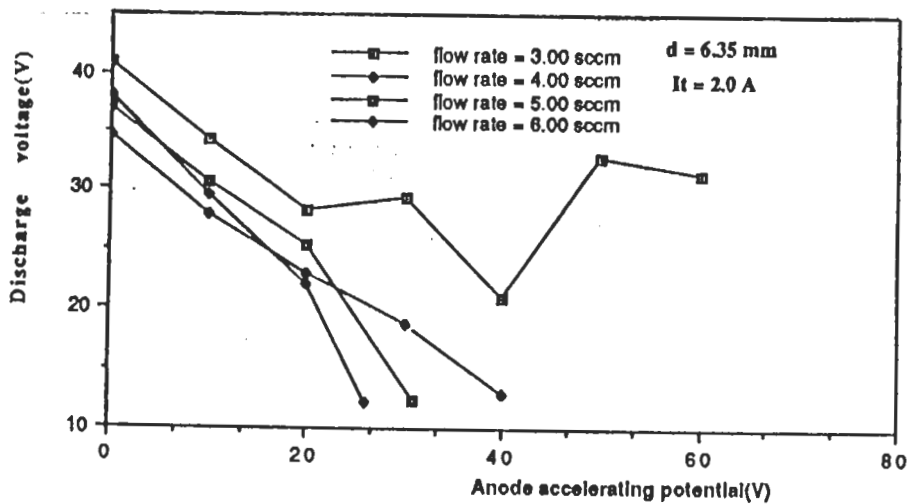


Figure 5.3 Discharge voltage vs. anode accelerating potential

Discharge potentials were significantly lowered for higher anode (collector) bias potential. At higher anode bias potentials the anode current leveled off and became essentially the total current (the keeper discharge current approached). The saturation current was a function of flow rate. Figure 5.4 shows the saturation effect as a function of flow rate. The potential associated with the saturation level varied from 20 V to 40 V. This is roughly the same as the accelerating anode potential of ion engines. From this analysis it may be determined that the higher flow rates would be profitable for power and discharge stability point of view only.

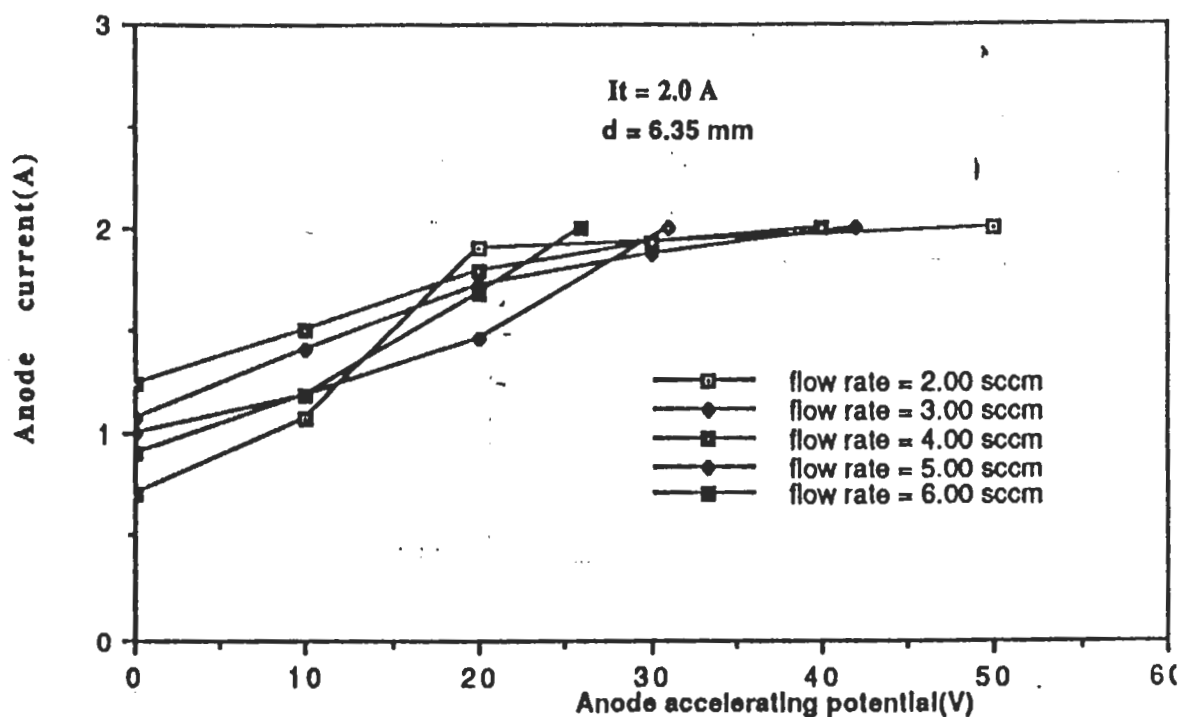


Figure 5.4 Level off potentials

B. NEGATIVE ANODE POTENTIAL RELATIVE TO KEEPER

The experiments described above were designed to study electron collection. Previous studies, such as those at Colorado State University, also look at ion production in the cathode by biasing the chamber walls negative with respect to the cathode. These experiments generally resulted in ion currents of $100 \mu\text{A} - 1 \text{ mA}$. Similar experiments at NPS yielded somewhat different results. The experimental arrangement was similar to part A, but the biasing arrangement was slightly changed so that the anode potential could be negative relative to the keeper. This configuration was useful for plasma diagnostic measurements. Figure 5.5 shows the bias configuration. For V_{ac} less than V_{kc} , the anode potential is negative with respect to keeper. This external bias affected the discharge substantially, due the large keeper hole diameter (1/4 inch). Figure 5.6 shows the discharge voltage vs. anode to cathode potential as functions of flow rate. The discharge potentials were raised as long as the potential of the anode was lower than keeper. Figure 5.7 shows anode current vs. voltage characteristic for a discharge current of 0.5 A. Even for -100 V , still there exists a small current possibly due to the electrons produced near the anode or electron emission from the negatively charged anode. For higher flow rate, this current was decreased. One possible reason is due to the higher gas molecular number density, and hence a higher collision frequency. For higher flow rate, the diffusion coefficient is decreased and energy transition through the inelastic collision is increased. Consequently fewer electrons arrive to the anode for same applied power. For further study of the current in the negative potential region, a movable Langmuir probe is needed.

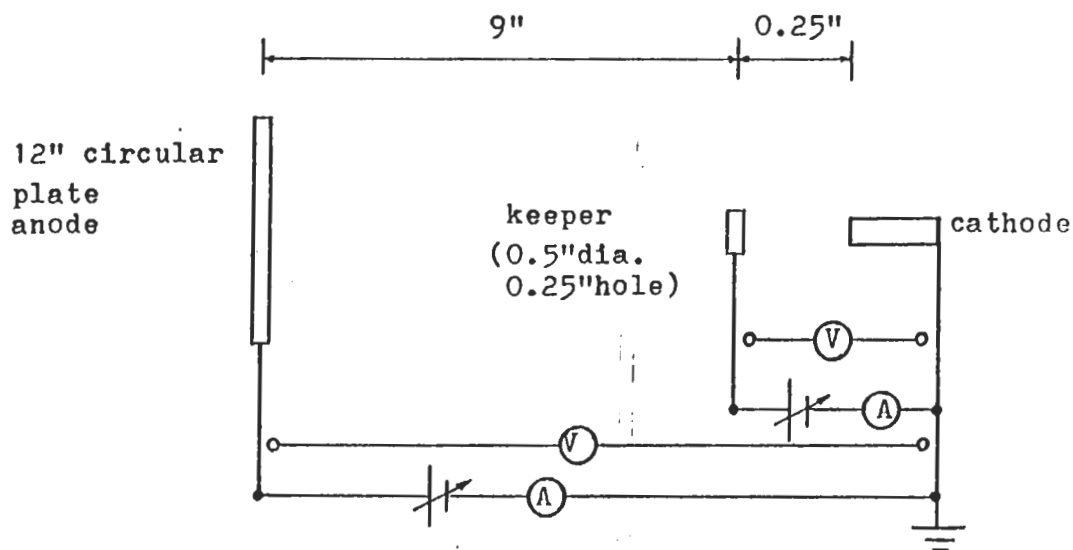


Figure 5.5 Bias configuration

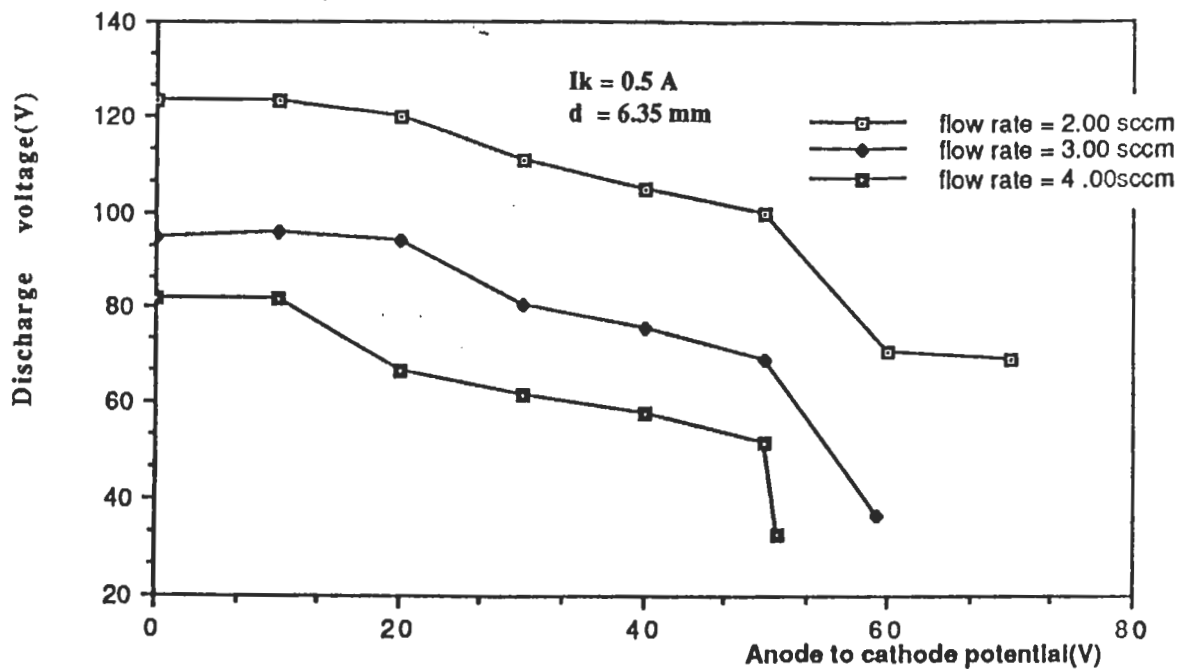


Figure 5.6 Discharge voltage vs. anode to cathode potential

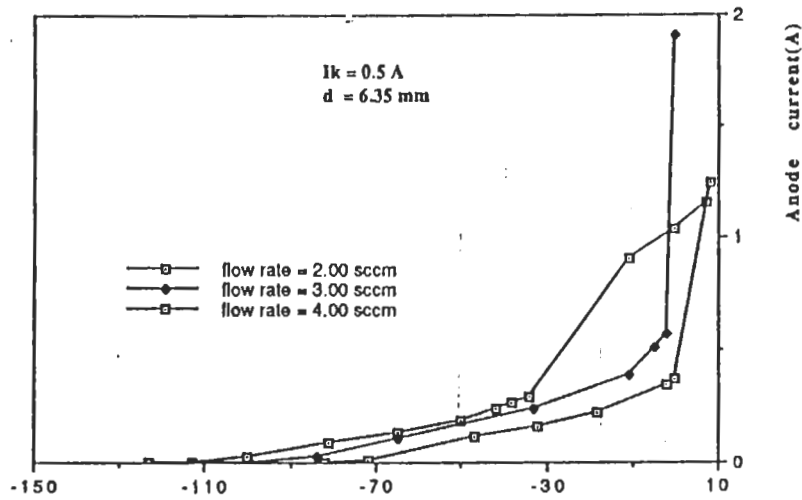


Figure 5.7 Anode current vs. potential

C. ANODE GEOMETRY DEPENDENCE

At the final stages of the experiment, the mesh type shield anode and 2 inch disk keeper with 1/8 inch hole were adopted as shown in Figure 5.8.

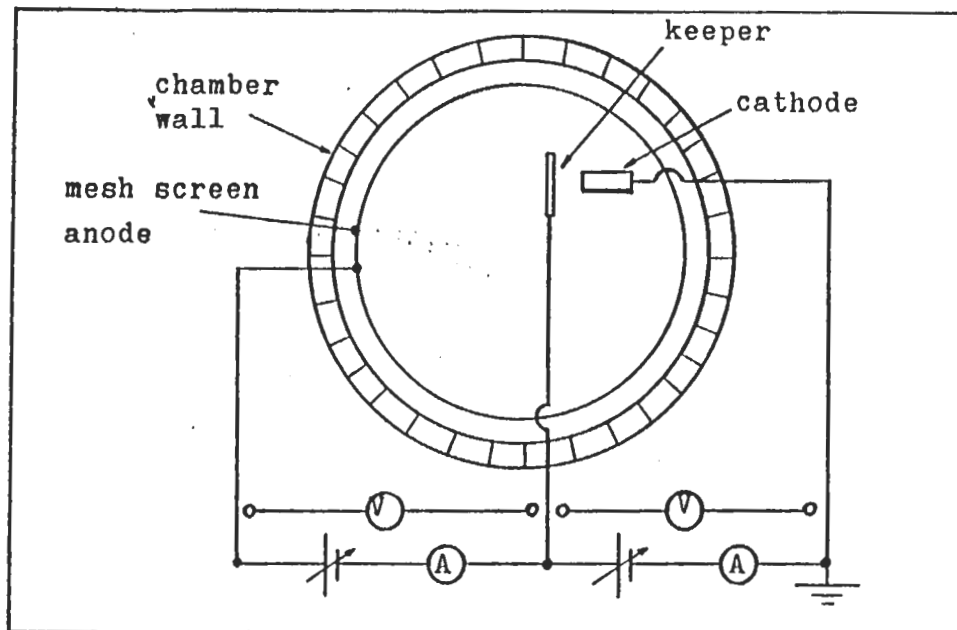


Figure 5.8 Mesh shield anode and vacuum chamber geometry

This mesh anode was employed as a screen to prevent the chamber wall from charging. Figure 5.9 and 5.10 show the discharge properties for a flow rate of 3.00 sccm and discharge current of 2.0 A. For the mesh anode, discharge characteristics were significantly changed. These changes were due to the change in anode electric field direction. In the previous case, the plate anode was located on the line from the cathode to keeper so that the superimposed anode electric field affected the discharge process. With the mesh anode, the electric field lines at the center of vacuum chamber was no longer directed along the discharge line. Thus, these field lines did not contribute to the discharge process for low anode potential. For V_{ak} greater than 40 V, the discharge mode changed to ignited mode when using a plate anode (collector). With the mesh anode, ignited mode required for V_{ak} greater than 80 V. The ignited discharge began in the region where the cathode was closest to the mesh. Consequently, an extra anode might be needed to force a large current from the hollow cathode system.

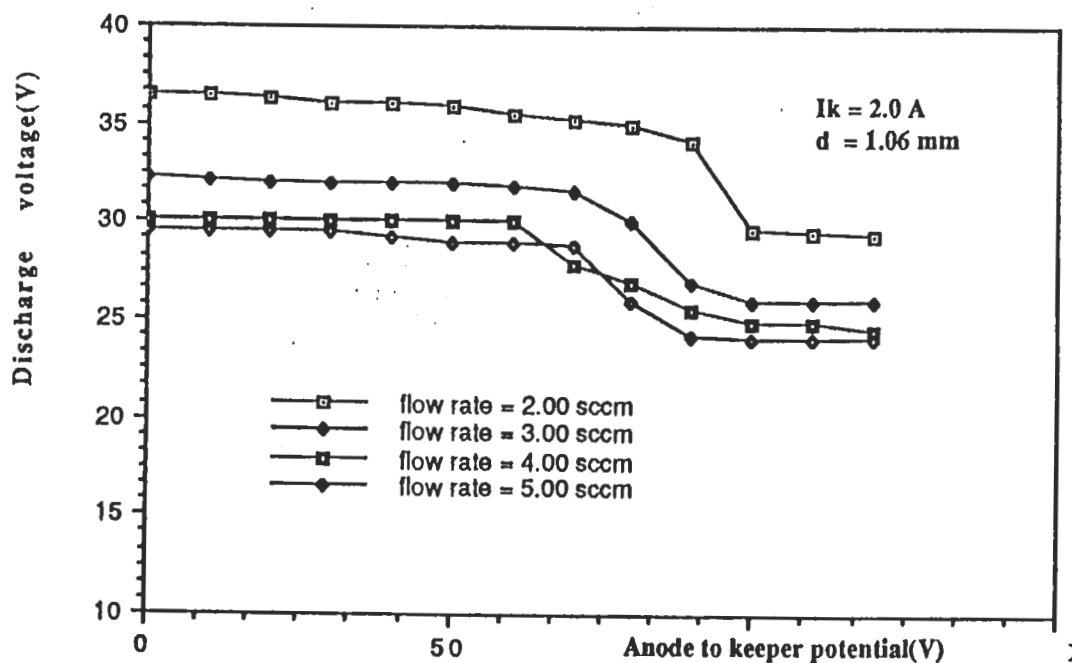


Figure 5.9 Discharge voltage vs. anode potential

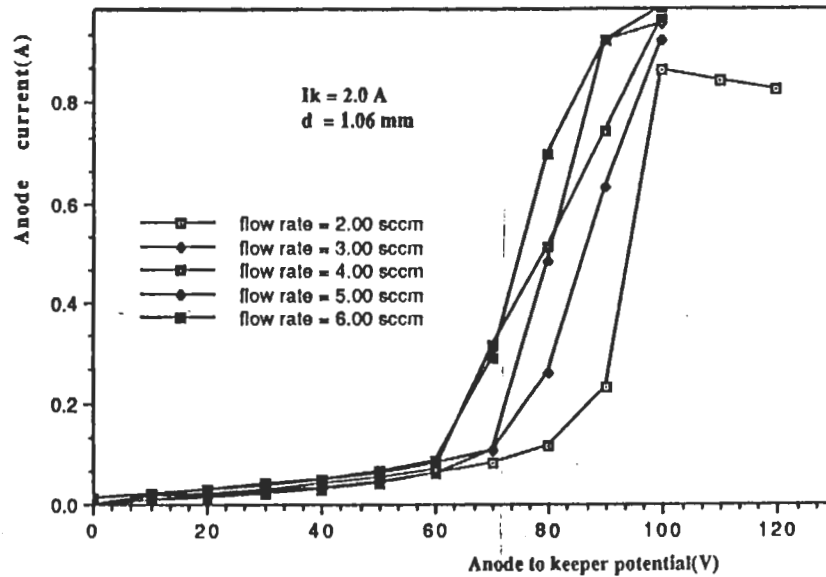


Figure 5.10 Anode current vs. anode potential

D. CATHODE TO KEEPER DISTANCE DEPENDENCE WITH MESH COLLECTOR

At the early stages, the cathode to keeper distance was fixed to about 6.35 mm (0.25 inch). The adjustable keeper was set to 1.06 mm and 2.12 mm. Figure 5.11 shows discharge voltage with respect to anode potential as a function of flow rate for a discharge current of 2.0 A. And Figure 5.12 shows a similar characteristic for a discharge current of 1.0 A.

A peculiar result was found at a flow rate 6.00 sccm. Figure 5.12 shows how at 1.0 A discharge current, there was a drop in the discharge voltage to 0.01 V at 53 V of anode to keeper potential. A beautiful cone shape discharge was produced. Apparently the keeper was effectively removed from the circuit. The distance effect was greater for lower discharge current levels. For lower discharge current and shorter distance, the discharge voltage increased.

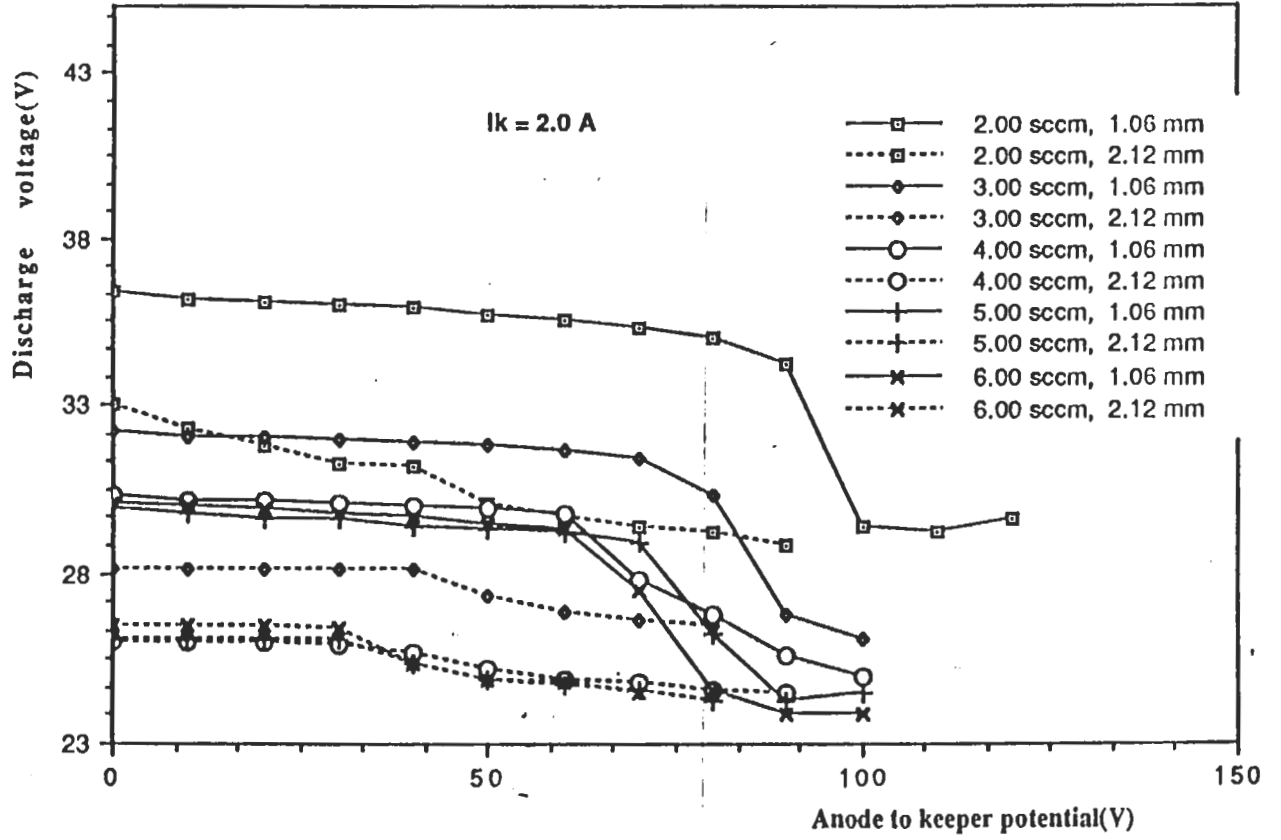


Figure 5.11 Discharge voltage vs. anode potential for $I_k = 2.0 \text{ A}$

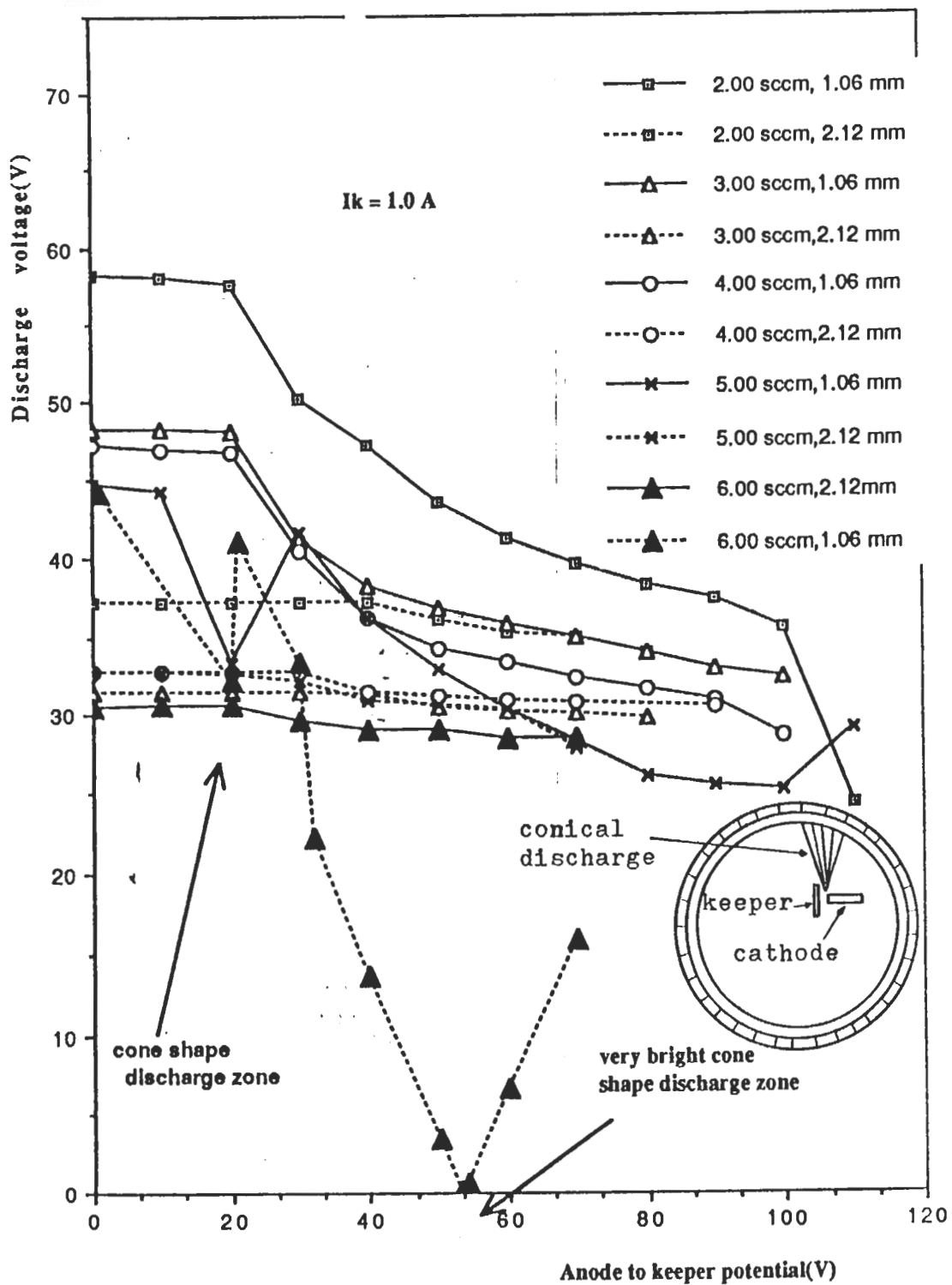


Figure 5.12 Discharge voltage vs. anode potential for $I_k = 1.0 \text{ A}$

E. HEATER DEPENDENCE

The heater dependence of the plasma characteristics was investigated for cathode to keeper distance 2.12 mm and discharge current 2.0 A and 1.0 A. The difference is in how the power necessary to maintain the discharge is provided to heat the thermionically emissive surface. For a discharge current of 2.0 A, the discharge was quite stable from heater currents from 2.0 A to 6.0 A. For heater currents less than 1.0 A, it was unstable. For a discharge current of 1.0 A, the discharge was generally unstable for heater current less than 5.0 A. The discharge characteristic depended strongly on heater temperature. Figure 5.13 shows the heater current dependence of the discharge for $d=2.12$ mm and a flow rate of 2.00 sccm. For a flow rate of 2.00 sccm and heater current of 6.0 A, the discharge voltage was half of it for heater current 2.0A.

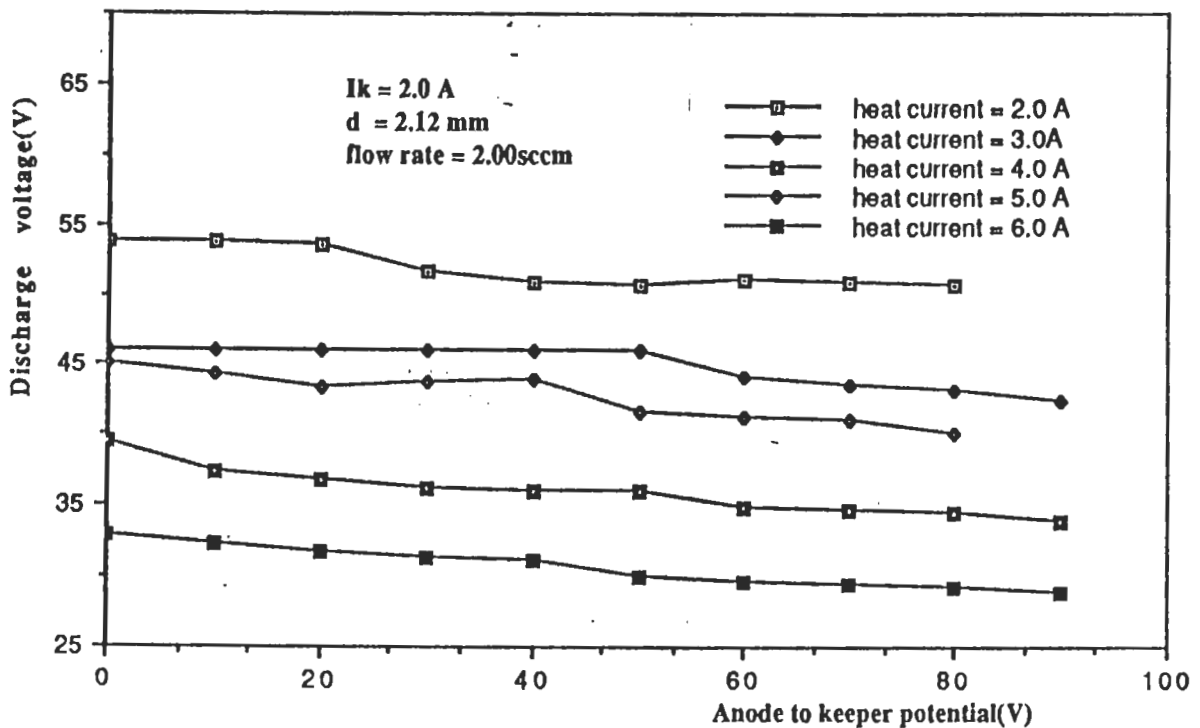


Figure 5.13 Discharge voltage vs. anode potential for flow rate 2.00 sccm

F. ELECTRON TEMPERATURE AND DENSITY

The fundamental plasma parameters such as electron temperature and density were determined by using a Langmuir probe (9.514 mm diameter) which was located 5 cm in front of the hollow cathode. Figure 5.14 shows the plots of probe current vs. potential as functions of flow rate and discharge mode. The collected current was limited by the capabilities of the voltage supply used for the Langmuir probe (further experiments should run with a small probe). In order to obtain electron temperature the logarithm of i_e was plotted against probe potential with respect to ground. Figure 5.15 and 5.16 show plots of $\ln(i_e)$ versus V_1 for both normal and ignited discharge modes. From the slopes of the linear portions of these curve, the electron temperature was calculated. It was found that the electron temperature for ignited mode was much higher than normal mode but the density was almost identical. Therefore, the radiation from the ignited mode was due to the excited atoms. Plasma density was calculated from the saturation current, surface area of Langmuir probe and electron temperature. Figure 5.17 and 5.18 are the summary of electron temperature and plasma density. [Ref. 17]

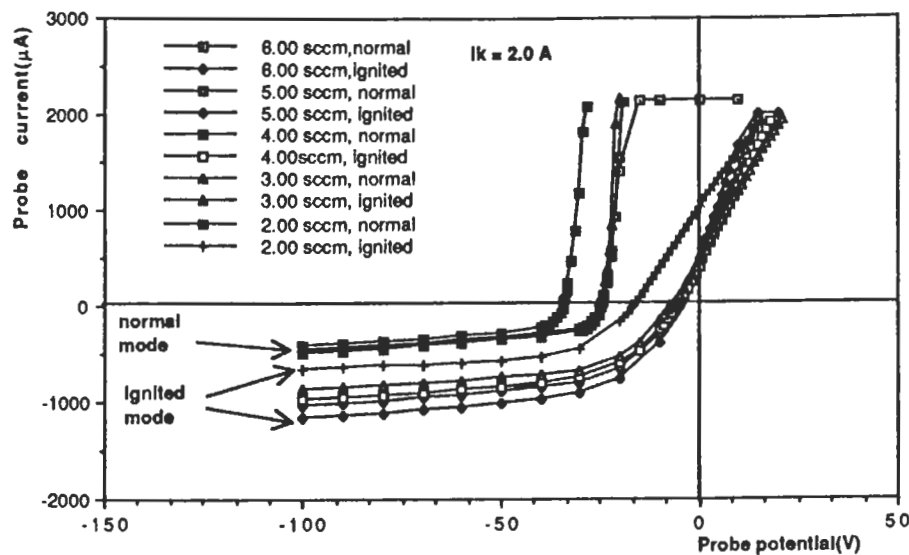


Figure 5.14 Probe current vs. potential for normal and ignited discharge mode

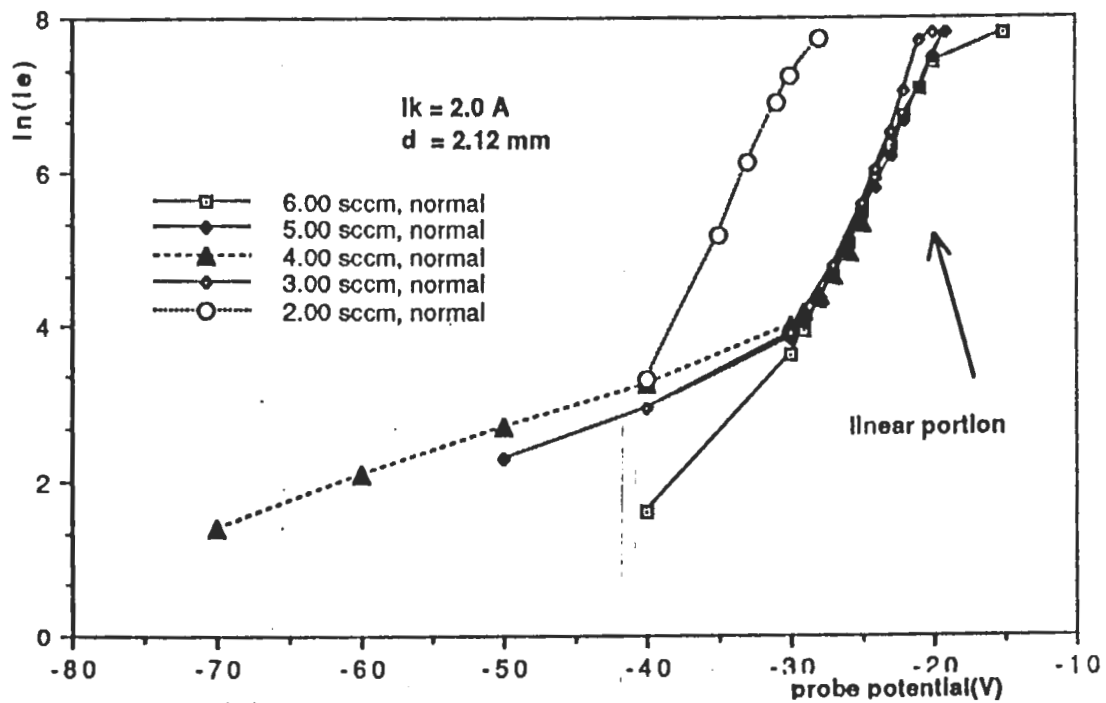


Figure 5.15 $\ln(i_e)$ vs. probe potential for normal discharge mode

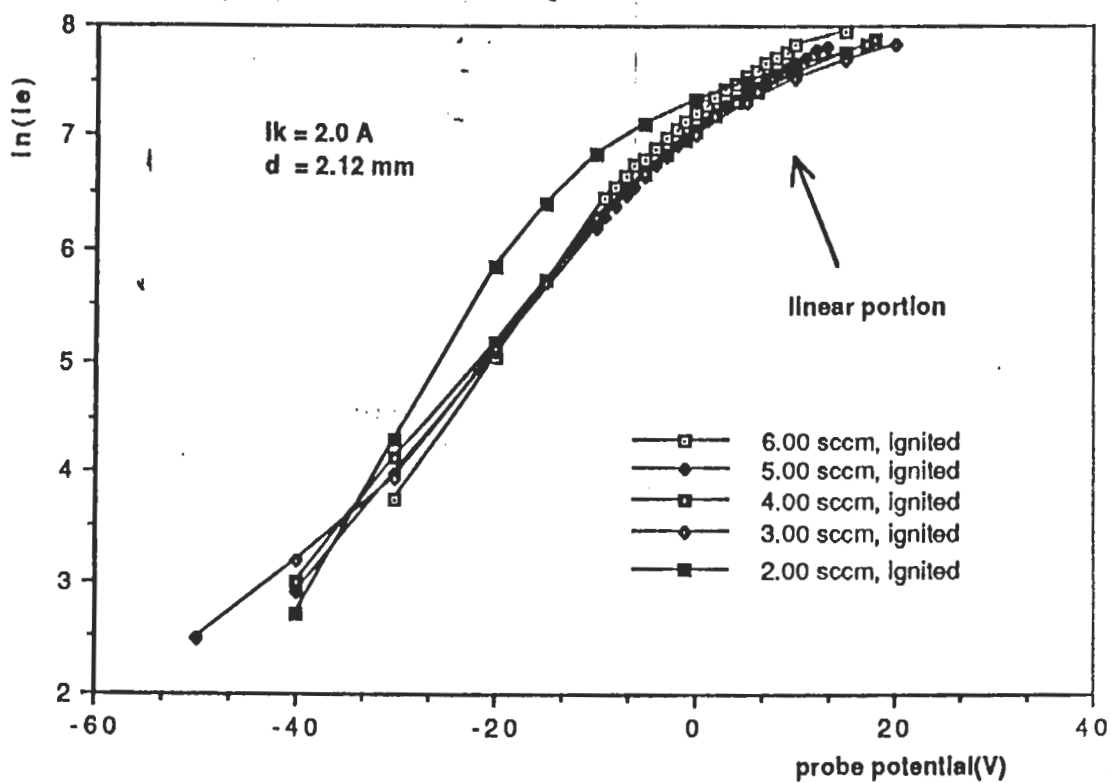


Figure 5.16 $\ln(i_e)$ vs. probe potential for ignited discharge mode

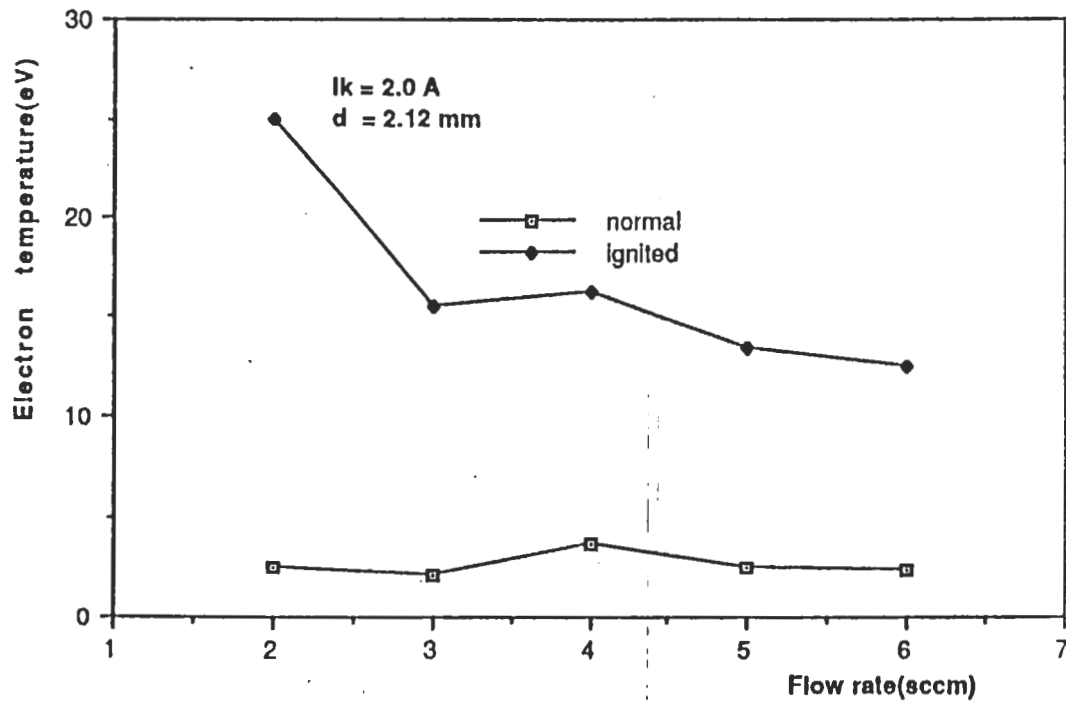


Figure 5.17 Summary of electron temperature

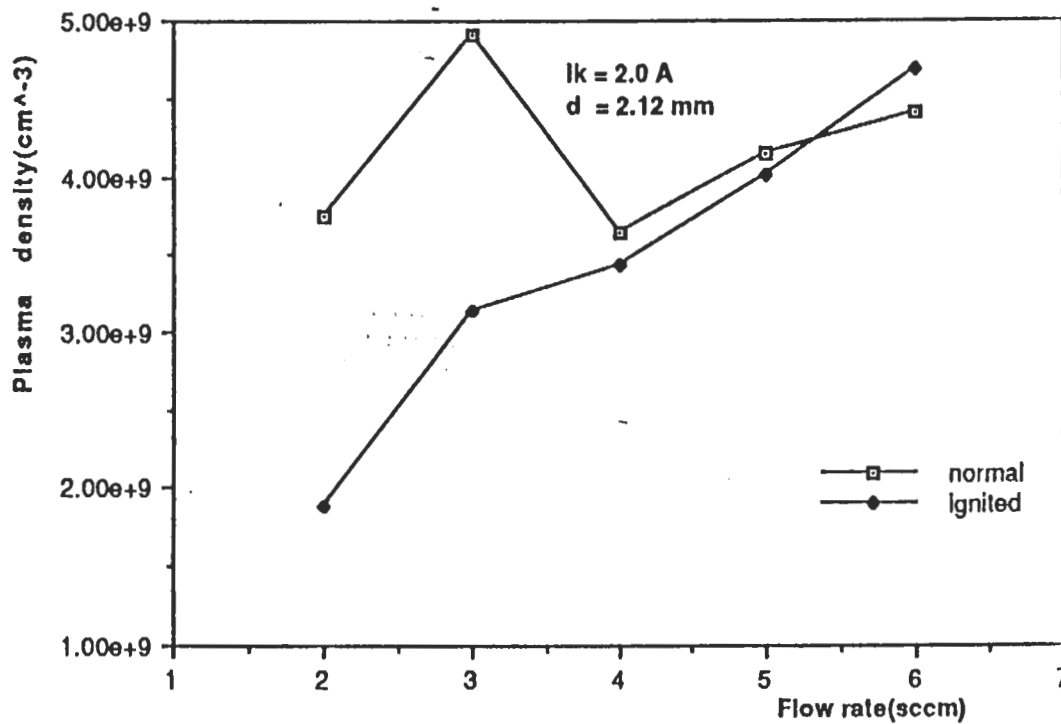


Figure 5.18 Summary of plasma density

G. OTHER RESULTS

1. Chamber pressure

Chamber pressure depended on discharge states and the speed with which keeper to cathode power was applied. In general, the pressure was higher when the discharge was on. This may have been due to higher gas temperature. If power was applied rapidly during ignition, the pressure was lowered for a moment (just a few seconds). If power was switched off quickly, the pressure increased then returned to normal pressure as shown in Figure 5.20. These transient pressure variations are not observed if power is varied slowly. This pressure variations might be a result of variations in the cathode tip temperature, and hence the orifice diameter. Also, the electric field causes ions to move upstream, impeding the gas flow via collision.

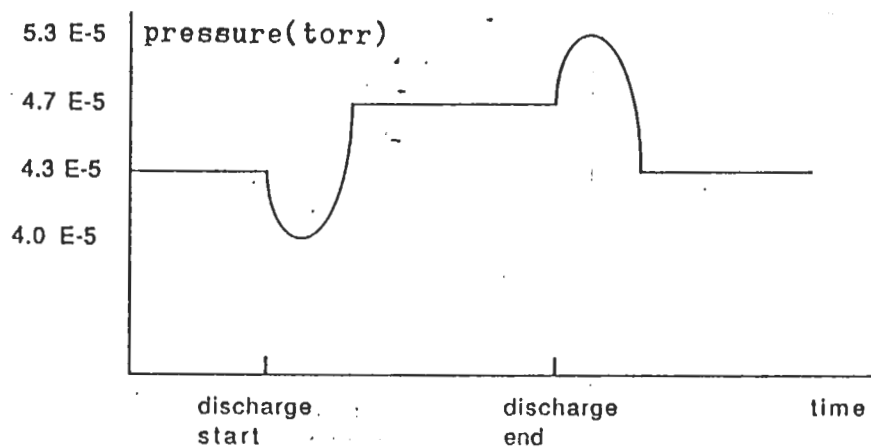


Figure 5.19 Chamber pressure variation with respect to discharge states

2. Back discharge

In the early phase of this experiments, the back (behind the plate anode) discharge (first reported by J. J. Thompson) was observed several times. It might be due to the pressure and potential difference between chamber wall and anode. But it could not be reproduced in the final stages of experiments.

3. Field – enhanced thermionic emission

A small amount of field – enhanced thermionic emission current, which initiates the discharge, was detected. It was a linear with respect to applied keeper to cathode potential as shown in Figure 5.21.

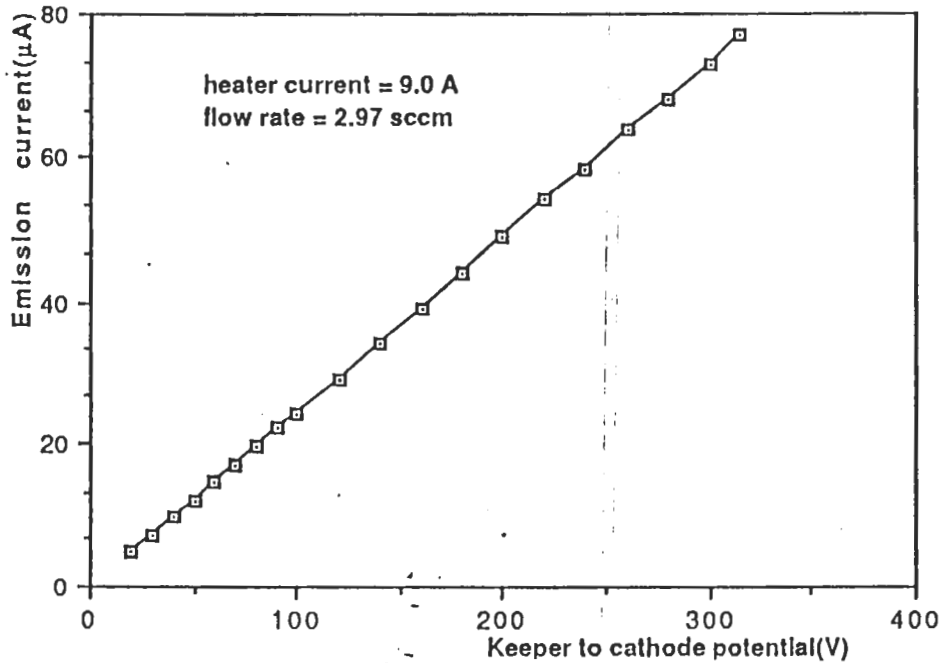


Figure 5.20 Field – enhanced thermionic emission current

This aspect of the discharge process has not been reported previously, in any reference we have been able to locate. This thermionic emission current must be a pre – cursor to ignition of the main discharge. It is tempting to speculate that the efficiency of this process ('resistance') determines the startability of the cathode.

VI. FURTHER WORK

Required further works to improve plasma diagnostic techniques are discussed here.

A. KEEPER

Now only keeper distance can be controlled for investigation of the distance effect. For further investigation of keeper shape effects, keeper with variable hole diameter should be considered.

B. LANGMUIR PROBE

For investigation of plasma density and temperature distribution with respect to space, a movable Langmuir probe is recommended.

C. ANODE

Unlike the plate anode, the mesh anode could not draw substantial current. This may be due to its geometry. To prevent this situation, it is recommended to split the mesh anode into several sections and apply potential by separate power supplies as shown in Figure 6.1.

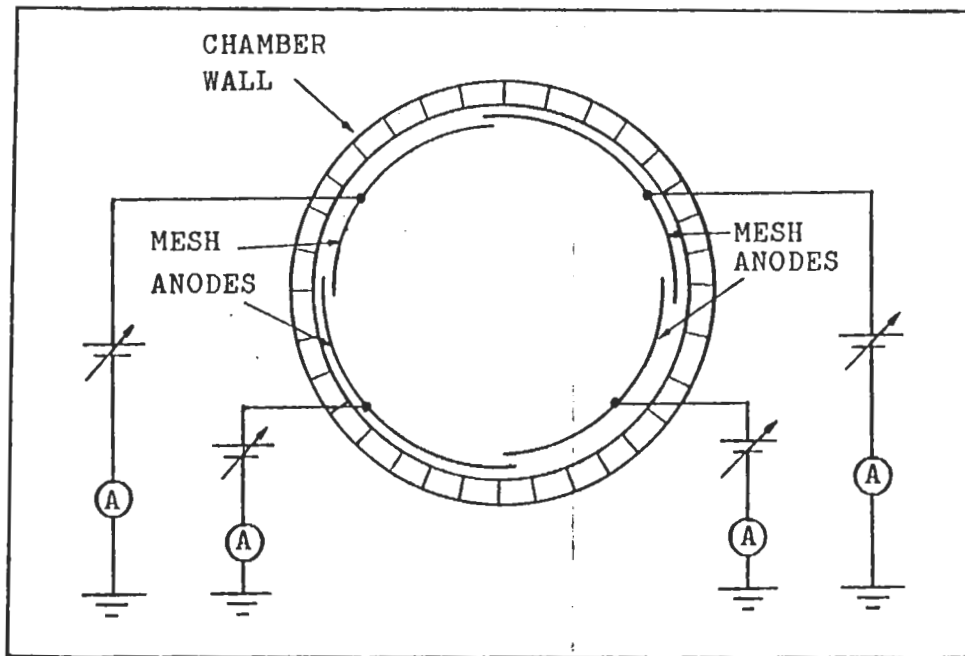


Figure 6.1 Split mesh anodes and bias configuration

VII. CONCLUSIONS

The experiments using a standard hollow cathode and argon gas agreed with the general discharge and plasma characteristics previously reported. Analysis of the data gave the following results:

- The electron temperatures were about 2 eV for normal discharge mode and about 10 eV for ignited discharge mode.
- The plasma density was the order of 10^9 cm^{-3} for both discharge modes.
- For the higher gas flow rate, the discharge was stable, predictable and lower power was required.
- The plate anode acted as a electron accelerator just as in an ion engine. The discharge reached a maximum current of potentials from 26 V to 50 V.
- For low anode potential the mesh screen anode did not contribute any significant effects to the discharge process, except for preventing the chamber wall from charging.
- For the mesh anode, very peculiar discharge phenomena such as a 0.01 V discharge voltage and conically shaped discharge were observed.
- For larger cathode to keeper distance and high flow rates, discharge potentials were lowered significantly.
- The current existing at negative anode potential suggests that some electrons were produced near the anode plate or electron emission occurred on the negative anode plate.

o. For higher heater current, the discharge voltage was lowered significantly.

LIST OF REFERENCES

1. Siegfried, D. E., " A phenomenological model describing orificed, hollow cathode operation " NASA CR – 165253.
2. Siegfried, D. E., and Wilbur, P. J., " A model for mercury orificed hollow cathodes: Theory and experiment " AIAA – 82 – 1889 Nov. 1982.
3. F. Llewellyn – Jones, " Ionization and breakdown in gases " Fletcher and Son Ltd. Norwich, 1966.
4. Charles Kittel and Herbert Kroemer, " Thermal physics " W. H. Freeman and company, 1980.
5. Glen R. Longhurst, " A method for obtaining electron energy density functions from Langmuir probe data using a card – programable calculator " AIAA Paper 81 – 0681.
6. A. Theodore Forrester, " Ion propulsion "
7. Francis F. Chen, " Introduction to plasma physics and controlled fusion vol. 1 " Plenum press, 1984.
8. V. K. Rawlin and E. V. Pawlik, " A mercury plasma – Bridge Neutralizer " NASA Lewis Research Center, Cleveland, Ohio.
9. C. H. Mount, G. Yamasaki, Walter Fowler and W, G, Fastie, " Compact far ultraviolet emission source with rich spectral emission " Applied optics vol. 16, March 1977.
10. Hamamatsu technical manual " Characteristucs and handling of hollow cathode lamp " Dec. 1984.
11. D. G. Fearn, Angela S. Cox, D. R. Moffitt, " An investigation of the initiation of hollow cathode discharge " Royal Aircraft Establishment Technical Report, 76054, 26 April 1976.
12. Spectra–Mat Inc. Technical manual, " Hollow cathode plasma source ", 1988.
13. A. von Engel, " Ionized gases " Oxford Clarendon press, 1965.
14. Ion Tech, Inc. Technical manual, " Hollow cathode manual HC – 252 ".
15. T. Dolan, " Fusion research, vol. II – experiments " Pergamon Press Inc., 1982.
16. H. J. Han, " Physical processes in hollow cathode gas discharge source " NPS, Dec. 1989.

17. C. M. Philip, " A study of hollow cathode discharge characteristics " RAE England, Nov. 1971.
18. John D. Williams, " Electrodynamics tether plasma contactor research " NASA CR – 182148, Jan. 1988.

INITIAL DISTRIBUTION LIST

- | | | |
|----|--|----|
| 1. | Defense Technical Information Center Cameron Station Alexandria, Virginia 22304-6145 | 2 |
| 2. | Library, Code 0142 Naval Postgraduate School Monterey, California 93943-5002 | 2 |
| 3. | Dr. R. C. Olsen Code 61Os Naval Postgraduate School Monterey, CA 93943 | 10 |
| 4. | Dr. S. Gnanalingam Code 61Gm Naval Postgraduate School Monterey, CA 93943 | 1 |
| 5. | Dr. K. E. Woehler Code 61Wh Naval Postgraduate School Monterey, CA 93943 | 1 |
| 6. | LT. Park, Young-chul, Korean Navy 180-00 Kyong Ki do Pyoung Taek city Segyo-dong, San 9 - 1 Seoul, Korea | 5 |
| 7. | Capt. Song, Tae-ik SMC 2686 NPS Monterey, CA 93943 | 1 |
| 8. | Maj. Han, Hwang-jin, Korean Army Songpa-ku Garak-dong Garak APT Seoul, Korea | 1 |
| 9. | Dr. Paul Wilbur Department of mechanical engineering Colorado State University Fort Collins, CO 80523 | 1 |